8-2024

Predicting the Ductility of Tungsten Based BCC Refractory High Entropy Alloys: A Computational Science Driven Study

Akshay Korpe
Clemson University, akorpe@clemson.edu

PREDICTING THE DUCTILITY OF TUNGSTEN BASED BCC REFRACTORY HIGH ENTROPY ALLOYS: A COMPUTATIONAL SCIENCE DRIVEN STUDY

A Thesis
Presented to
the Graduate School of
Clemson University

In Partial Fulfillment
of the Requirements for the Degree
Master's of Science
Mechanical Engineering

by
Akshay Korpe
August 2024

Accepted by:
Dr. Enrique Martinez Saez, Committee Chair
Dr. Cheng Sun
Dr. Garrett Pataky

Abstract

Bcc refractory high entropy alloys (HEAs) are a relatively new category of metallic alloys that promise excellent irradiation resistance and strength retention at high temperatures but exhibit brittle behavior at room temperatures limiting their formability. Understanding the deformation mechanisms and predicting their ductility at room temperature is a topic of interest in contemporary research.

In this work, multiple independent ductility criteria for quantifying the ductility of these HEAs were studied, calculated and compared using Density Functional Theory (DFT) calculations and continuum mechanics frameworks. These ductility parameters were calculated for various W-Ta-Cr-V alloys and the trends were analyzed for each criteria for dependence on the concentrations of the alloying elements.

The correlations between the analytical Rice model with the other approximate and phenomenological models were analyzed to investigate their viability to serve as computationally inexpensive surrogate models for screening potentially ductile HEAs from a large compositional space without performing DFT intensive computations required by the Rice model.

In order to further improve computational efficiency, a predictive cluster expansion model was developed using the DFT datasets generated for the W-Ta-Cr-V alloys to predict the Ground state energies of the HEAs. This framework is discussed for viability in accurately predicting the Free Surface Energies (γ_{SURF}) , Unstable Stacking Fault Energies (γ_{USF}) and elastic constants, and by extension, the ductility of these alloys.

Dedication

This research project is dedicated to my mom, dad and my brother back in my hometown India. I am able to work towards my dreams today because of your unconditional love, support and sacrifices. I love you all.

To my research advisor Dr. Enrique Martinez Saez for your unwavering support and lots and lots of patience with me throughout this project. I learned a whole lot more than the scope of this research from you.

To my friends Dr. Indrayani Jadhav, Manas Phanse, Cheran Teja Dumpati, Sarvesh Tambat, Gabriella Knight and Anushka Prapanna. It would not have been as fun without you guys.

Acknowledgments

I want to thank my research advisor Dr. Enrique Martinez Saez for introducing me to the domain of this research and being a resolute part of it. It is only due to his expertise and profound inputs that this research was possible.

I would also like to thank members of my thesis committee, Dr. Garrett Pataky and Dr. Cheng Sun, for their constructive feedback and inputs which helped me improve and refine the quality of this research.

I would like to mention my research group which consists of bright and motivated people in the domain of my research. It was great help and a wonderful experience to be able to collaborate with them throughout this journey.

Finally, I want to express the deepest gratitude towards Clemson University for providing the facilities and infrastructure needed for the completion of this research.

Table Of Contents

List of tables

List of figures

Chapter 1

Introduction

1.1 Overview and history of High Entropy Alloys

High Entropy alloys (HEAs), also widely known as Multi-Principal Element Alloys (MPEAs) are a relatively new category of metallic alloys which typically consist of five or more elements in non-dilute proportions. The term high-entropy alloys was first coined by Jien-Wei Yeh.[1] Generally, a typical metal alloy consists of one or two elements in major proportions, with other elements in relatively small proportions. High entropy alloys differ from traditional alloys when it comes to these elemental proportions. Many definitions define HEAs as alloys with multiple principal alloying elements in significant proportions. Other definitions try to classify them based on the peculiar physical properties that are observed in them. This means that there is no universally accepted definition for them, although there are a few widely accepted ones.

One definition recognizes as multi-principal element alloys with 5 or more elements with a concentration range of 5% - 35%[4] , although multiple alloys that do not conform to this definition are accepted as HEAs in multiple research studies.[6]

Another widely accepted definition is what defines HEAs as alloys that possess a set of peculiar physical properties coined as the ‘Four core effects’[5]. According to this definition, all HEAs exhibit these four peculiar properties :

1) High entropy effect :

A typical solid solution has 3 competing solid states, i.e. elemental phase, intermetallic compounds phase and solid-solution phase.[5] The elemental phase is an infinite solid solution of one element.In an intermetallic compound phase, the stoichiometric compound has a specific lattice structure. Solid-solution phases are formed when there is a random and complete mixing of the constituent elements in significant proportions in any one of the crystal structures.

As the number of atomic species increases, the enthalpies of mixing for solid solutions and for intermetallics start to get closer to each other.[5] Also, as the atomic species increases, the entropy of mixing gets higher for solid solutions as compared to intermetallics due to the high number of microstates possible. This indicates that the solid solution will have a lower Gibbs free energy than the intermetallic phases, especially at elevated temperatures. This results in a bias towards the formation of solid solution phases and this phenomenon is called the high entropy effect.

It should be noted that this assumes the atomic radii as well as the bonding energies to be roughly equal. However, many HEAs tend to precipitate into multiple intermetallic phases and exhibit short range ordering especially at lower temperatures.[34]

2) Sluggish diffusion effect :

Due to the nature of HEAs, each lattice site is surrounded by different atomic species. This gives rise to a large fluctuation in the potential energies of these lattice sites. It is theorized that the lattice sites with low potential energies can act as traps for vacancy

mobility and hence result in a sluggish diffusion and higher activation energies[5].

This may not always be the case though as there are many studies that show that refute this effect[35].

3) Severe lattice distortion :

   Due to such differences in the atomic species, each lattice site has an atom with a variety of bond energies and atomic radii. This along with the tendency of phase separation gives rise to high degrees of stresses within the crystal and causes it to become severely distorted. This causes the material to undergo solid solution hardening thus increasing the hardness and also results in a reduction in the thermal conductivity.[5]

4) Cocktail effect :

   Due to the large fluctuations in the occupancy of the lattice sites in HEAs, both on the atomic and crystalline levels, the properties of these alloys are often a concoction of many properties on the microscale.[5] This inconsistent behavior of HEAs due to multiple phase formations and atomic interactions even for very small stoichiometric changes is coined as the ‘cocktail effect’.

There are other proposed classifications of HEAs that only consider the solid solutions without any intermetallic phases as true HEAs as the intermetallics will reduce the mixing entropy.[36] In this work, we consider a four element single phase bcc quaternary HEA consisting of the refractory elements W, Cr, V and Ta.

1.2 Overview of bcc High Entropy Alloys

Refractory Body Centered Cubic (BCC) HEAs which are also commonly referred to as Refractory Multi-Principal Element Alloys (RMPEAs) are a class of HEAs consisting mainly of W, Mo, Cr, Nb, V and Ta, and are known to show desirable properties such as excellent strength retention at elevated temperatures(1000 °C and above), outstanding irradiation resistance[37], high melting temperatures and a weak dependence of their yield strength to the temperature (about 400 GPA at 1600 °C). This makes them desirable for high temperature applications. However, many of these alloys are known to possess poor ductility at room temperature, limiting their formability and applications.[6,7]

Most experimental work towards the ductility of HEAs has been done for compression. These tests show low ductility in compression as well. This leads to the conclusion that the mode of failure in this class of alloys is not related to ductile mode of failure, but fracture. Also, the pure refractory bcc metals (W, Nb, Mo, Ta, Cr, V) all show a sharp temperature brittle to ductile transition which means that this behavior is not just peculiar to HEAs.[6]

These bcc refractory HEAs, known to show promising potential for excellent mechanical performance at elevated temperatures both in computational and experimental studies, have put forward a new challenge in the field of computational material science due to their extremely large compositional space, especially in the area of Density Functional Theory (DFT) methods which are already computationally expensive even for pure elements and dilute alloys. The main challenges in this domain of research are hence the limited datasets available due to the inherently computationally expensive nature of DFT methods. This along with the increasing industrial interest in the formability and

machinability of these HEAs has given rise to an urgent need for developing frameworks to predict the ductility of these alloys at room temperature.

In this work, we have compared 6 widely used ductility criteria for various concentrations of W-Ta-Cr-V based bcc HEAs.Out of these, the Rice model is an analytical solution that has a well defined theoretical basis. The other 5 models are either an approximation of the Rice model or are phenomenological in nature. These non-analytical models are much more computationally efficient but are expected to have lower accuracy. The correlation between the concentrations of the base elements and the ductility of the alloys is studied. The correlation between the results from all the non-analytical criteria are also analyzed with respect to the Rice model which is by far the most accurate but computationally most expensive.This has been done in an attempt to formulate a surrogate model for the screening of the potentially ductile alloys from a large compositional space of HEAs which is much more computationally efficient than the Rice model without a significant loss in accuracy. The idea is that the ductility of the screened alloys can then be more accurately predicted using the Rice model which can result in much higher computational efficiency overall. In order to further improve the computational efficiency, a Cluster Expansion model is set up for predicting the ground state energies using the DFT datasets generated. The potential for this model to further predict other intrinsic properties such as the Free Surface Energies (γ_{SURF}) , Unstable Stacking Fault Energies (γ_{USF}) and elastic constants, and by extension, the ductility of these alloys is also discussed to help set up a ductility prediction model without carrying out the computationally expensive DFT calculations.

Chapter 2

Methodology

2.1 Density Functional Theory calculations

2.1.1 Generation of bcc HEA supercells

In this study, the crystal structures for performing DFT calculations were generated using Atom, Molecule, Material Software Kit (Atomsk)[13]. Crystals containing pure bcc refractory elements Tungsten (W), Tantalum (Ta), Chromium (Cr) and Vanadium (V) as well as HEAs containing binaries, terneries and quarternaries containing these four elements in varying concentrations were generated. Moreover, for each concentration, multiple random configurations were generated to simulate the randomness one might expect in nature.

Each crystal structure contains either 108 or 216 atoms in total and is generated as a rectangular prism. The structure is generated in a non-standard orthogonal basis vectors 6[111] x 2[-1-12] x 3[1-10] to make calculations in the most active fracture planes easier. All the structures are generated starting with a pure W crystal and then substituting W atoms with other atoms in a random fashion. These bulk structures are then relaxed using DFT. A total of 33 different alloys based on the concentrations of the base atoms were studied and for each alloy, an average value of 10 random configurations was calculated and selected to model for randomness in nature.

2.1.2 Ground State Energies for the bulk structures :

This study made use of the Vienna Ab initio Simulation Package (VASP)[14,15,16,17,18] to perform the DFT simulations. The structures are relaxed to the ground state by using ISIF = 3 that allows for the deformation of the box to reach 0 pressure and EDIFFG = -0.005 as the tolerance in the atomic forces. The energy of the ground states is the energy of these relaxed structures.

2.1.3 Free Surface Energies (γ_{Surf}) :

The free surface energies for all the bulk structures was calculated. The free surfaces that were studied were the [1-10] and [-1-12] planes. They were created by adding a buffer of 10 A° normal to the plane in the relaxed bulk structure using Atomsk. Then the new structure with free surfaces is relaxed to ground state again, but this time using ISIF = 2 (The allowed degrees of freedom include relaxation of the forces with the cell shape and volume). The global energy cut-off was EDIFF = 0.0001 eV. This structure in its relaxed state will give us the energy of the bulk structure with a free surface.

The free surface energies are the difference between the relaxed state energies of the structure with a free surface and the bulk structure without the free surface. This difference was averaged out for all the configurations for each concentration to get an average value of free surface energy to simulate the randomness expected in HEAs. The energies are then divided by the areas of the free surfaces that are generated to give us free surface energies in the standard units eV / $A°^2$.

The free surface energy is given by the following equation[7] :

$$\gamma_{hkl} = E(slab)_{hkl} - n(slab) \cdot E(bulk)_{hkl} / 2 \cdot A(slab) \quad \text{(i)}$$

Where,

γ_{hkl} is the free surface energy of plane hkl

$E(slab)_{hkl}$ is the total slab energy

$E(bulk)_{hkl}$ is the energy per atom of the bulk structure

n(slab) is the number of atoms in the slab

A(slab) is the surface area of the slab

A total of 33 different alloys based on the concentrations of the base atoms were studied and for each alloy, an average value of 10 random configurations was calculated and selected to model for randomness in nature.

2.1.4 Unstable Stacking Fault energies (γ_{USF}) :

The Unstable Stacking Faults energies for all the bulk structures were calculated. The relaxed bulk structures with free surfaces were used. For each concentration, a weighted Unstable Stacking Fault was added to the plane of the free surfaces at the center of the structures. In the present work, for the sake of simplification, the γ_{USF} is treated as the GSF energy at a fixed shift distance that equals to the length of 1/4 [111] instead of interpolating the maximum point of the GSF energy curve as the function of the shift distance. Another measure taken for the sake of simplification is that only one [110] plane was considered instead of the average of all the different planes that exist parallel to that plane. To offset this, an average of multiple planes was taken for at least 10 different configurations for each composition.

The γ_{USF} is given by using the following equation :

$E(\gamma_{USF}) = E(bulk) - E(\gamma_{USF}$ ¼[111]) (ii)

Where,

$E(\gamma_{USF})$ is the unstable stacking fault energy

E(bulk) is the relaxed ground state energy of the bulk system

$E(\gamma_{USF}$ ¼[111]) is the relaxed energy of the system after inducing a stacking fault of length ¼ [111]

The structure was then relaxed only in the direction normal to the free surfaces using ISIF = 2 (The forces are relaxed but the cell shape and volume remain fixed).The global energy cut-off was EDIFF = 0.0001 eV. Also, this relaxation was only allowed in the direction normal to the plane of the free surface which is perpendicular to the induced Unstable Stacking Fault. This was achieved using the Selective Dynamics feature in VASP to fix the relaxation in the directions in-plane of the free surface. The bulk structure with free surfaces was used instead of the original bulk structure for the calculations because the buffer added to generate the free surface makes sure that only one stacking fault was added instead of 2 due to the intrinsic continuous boundary conditions of VASP. If no buffer was added, there would be 2 stacking faults induced, one as intended at the center of the supercell and another at the edge due to the continuous boundary conditions in VASP.

The γ_{USF} energy is then calculated by calculating the difference between the bulk structure with the free surface and the stacking fault and the bulk structure with only free surface. This energy was then divided by the areas of the free surfaces that are generated to give us free surface energies in the standard units eV / $A^{\circ 2}$. A total of 33 different alloys based on the concentrations of the base atoms were studied and for each alloy, an average value of 10 random

configurations was calculated and selected to model for randomness in nature.

2.1.5 Elastic Constants

The Elastic constants calculations were carried out using VASPKIT[19]. The relaxed bulk structures were used and VASPKIT was used to apply strains and calculate the Elastic Constants using the strain energies. A total of 33 different alloys based on the concentrations of the base atoms were studied and for each alloy, an average value of 10 random configurations was calculated and selected to model for randomness in nature.

Every relaxed bulk structure was approximated to a cubic bcc crystal structure by applying symmetries in VASPKIT and hence only 3 independent elastic constants were to be determined (C_{11} , C_{12} and C_{44}). These structures were subjected to normal and shear strains in the range of (-0.015, -0.01, -0.005, 0, 0.005, 0.010, 0.015) and the strained structures were relaxed again using ISIF = 2 and the ground state energies were fitted to the square of the applied strains to calculate the elastic constants (C_{11} , C_{12} and C_{44}). The elastic constants for the pure elements were verified on the Materials Project[20] website and the results are found to be accurate. The theoretical basis for the DFT calculations for calculating the elastic constants is as follows :

For cubic crystals with all symmetries, we have 3 independent elastic constants in the stiffness matrix. Since all alloys studied in this work are based on a W lattice which is known to have a cubic lattice from experimental evidence[20], we assume all of them to be cubic. Hence, we have a stiffness matrix with only C_{11} , C_{12} and C_{44} .

The generalized Hooke's law is given by :

$$\boldsymbol{\sigma}_i = C_{ij} \,.\, \boldsymbol{\varepsilon}_j \,, \qquad \text{(iii)}$$

Where,

$\boldsymbol{\sigma}_i$ = stresses in the Voigt notation

C_{ij} = stiffness constant in Voigt notation containing only C_{11} , C_{12} and C_{44} for cubic crystals

$\boldsymbol{\varepsilon}_j$ = strains in Voigt notation

The Elastic Energy of a solid under strain under the harmonic approximation (no thermal expansion) is given by :

$$\Delta E(V,\{\boldsymbol{\varepsilon}_i\}) = E(V,\{\boldsymbol{\varepsilon}_i\}) - E(V_0,0) = V_0 / 2 \,.\, \sum^{6}_{i,j=1} C_{ij} \,.\, \boldsymbol{\varepsilon}_j \,.\, \boldsymbol{\varepsilon}_i \,, \qquad \text{(iv)}$$

Where,

V = volume after strain

V_0 = original volume

$\Delta E(V,\{\boldsymbol{\varepsilon}_i\})$ = elastic energy

$E(V,\{\boldsymbol{\varepsilon}_i\})$ = total energy after application of strain

$E(V_0,0)$ = total energy without any strain

Let $\boldsymbol{\delta}$ be the strain value applied. First, a triaxial normal strain ($\boldsymbol{\delta}$, $\boldsymbol{\delta}$, 0, 0, 0, 0) is applied to the undeformed perfectly cubic crystal. The Elastic energy is therefore given by :

$$\Delta E = V_0 / 2 \,.\, (C_{11}\boldsymbol{\varepsilon}_1\boldsymbol{\varepsilon}_1 + C_{11}\boldsymbol{\varepsilon}_2\boldsymbol{\varepsilon}_2 + C_{12}\boldsymbol{\varepsilon}_1\boldsymbol{\varepsilon}_2 + C_{12}\boldsymbol{\varepsilon}_2\boldsymbol{\varepsilon}_1) = V_0 \,.\, (C_{11} + C_{12}) \,.\, \boldsymbol{\delta}^2 \qquad \text{(v)}$$

Similarly,

On application of triaxial shear strain (0, 0, 0, $\boldsymbol{\delta}$, $\boldsymbol{\delta}$, $\boldsymbol{\delta}$), the elastic energy is given

by :

$$\Delta E = V_0 / 2 \, . \, (C_{44}\boldsymbol{\varepsilon}_4\boldsymbol{\varepsilon}_4 + C_{44}\boldsymbol{\varepsilon}_5\boldsymbol{\varepsilon}_5 + C_{44}\boldsymbol{\varepsilon}_6\boldsymbol{\varepsilon}_6) = 3 \, . \, V_0 / 2 \, (C_{44}) \, . \, \boldsymbol{\delta}^2 \qquad \text{(vi)}$$

Finally,

On application of triaxial shear strain ($\boldsymbol{\delta}$, $\boldsymbol{\delta}$, $\boldsymbol{\delta}$, 0, 0, 0), the elastic energy is given by :

$$\Delta E = 3 \, . \, V_0 / 2 \, (C_{11} + 2 \, . \, C_{12}) \, . \, \boldsymbol{\delta}^2 \qquad \text{(vii)}$$

For strain values $\boldsymbol{\delta}$ in the range of (-0.015, -0.01, -0.005, 0, 0.005, 0.010, 0.015) , we can fit the elastic energies per unit volumes with the squares of the applied strains to get the elastic constants C_{11} , C_{12} and C_{44} .

Here you have 2 equations for 3 unknowns. You are missing 1 equation.

2.1.6 Cluster expansion for predicting ground state energies :

The Alloy Theoretic Automated Toolkit (ATAT)[27] was used to develop a predictive Cluster Expansion (CE) model for the ground state energies of the alloys. It takes in the atomic species and positions from a perfect lattice file and predicts the ground state energy after relaxation of the structure.

The CE is an analytical framework that correlates the energy of a crystal structure with the atomic clusters through correlation functions. The formulation is of the form :

$$\hat{E} = J \, . \, X, \qquad \text{(viii)}$$

Where,

$\hat{E}$ is a vector representing the energies of the corresponding clusters

in the vector X.

X is a vector containing information about the clusters that are taken into account for the cluster expansion.

J is the correlation matrix that contains the correlation coefficients between the vectors $\hat{E}$ and X.

Under ideal conditions, the vector X contains every possible cluster in the supercell and $\hat{E}$ contains the corresponding energies. This would give a perfect correlation functional matrix J that can accurately predict the energies of any structure. However, since it is almost impossible to consider all the possible in complex structures such as HEAs, the effective clusters chosen in X can result in inaccurate predictions. To validate the effective clusters, ATAT has a built-in algorithm that gives out the Cross Validation Score (CV score). The CV score is calculated as :

$$CV = (1/n \cdot \sum_{i=1}^{n} (E_i - \hat{E}_i)^2)^{0.5} \quad \text{(ix)}$$

Where,

n is the number of atoms per unit cell,

E_i is the energy of cluster i ,

$\hat{E}_i$ is the predicted energy of cluster i.

The key to setting up a good cluster expansion is to minimize the CV score by selecting the optimum number of clusters as it is also quite susceptible to overfitting. ATAT has built in algorithms that can generate new structures as well as warn the user about overfitting.

2.2 Ductility models

Many studies have been carried out in an attempt to set up a theoretical framework for predicting the ductility of HEAs using computational techniques. Most of them rely on intrinsic parameters calculated using DFT techniques. Some of these criteria are used in this work to develop a CE model for the prediction of the ductility of W-Ta-V-Cr based refractory HEAs. Following is a summary of all the ductility criteria studied and used in this research :

1. Ductility index D using Rice model[6] :

   Bcc HEAs are known to exhibit low ductility both in tension as well as compression. This suggests that the mode of failure in these alloys is connected to fracture and not the traditional ductile failure mechanisms like necking. These alloys are also known to show a relatively sharp brittle to ductile transition with increasing temperature. This applies to pure bcc refractory metals like W, Ta, Cr and V as well, suggesting that this brittle behavior exhibited by the bcc HEAs have mechanisms unrelated to the typical HEA characteristics like severe lattice distortions and the cocktail effect.

   It is postulated that the intrinsic ductility in bcc refractory elements is governed by the fracture behavior at crack tip during fracture. This model assumes that the intrinsic fracture behavior of a material is governed by the competition between the dislocation emission and the brittle cleavage propagation at an atomistically sharp crack tip. A material is intrinsically ductile if the dislocation

emission at the crack tip occurs at stress intensity factor K_e at the crack tip occurs prior to the cleavage occurring at stress intensity factor K_c at crack tip. The dislocation emission blunts the sharp crack tip and enables the onset of ductile mechanisms of failure (void nucleation, growth and coalescence ahead of the crack tip). If the cleavage occurs first, the crack remains sharp and continues to propagate.

Most experimental studies of ductility of bcc HEAs are conducted under compression due to the industrial interest in formability of these alloys as well as due to the large number of specimens required for performing tensile tests.There is also research evidence suggesting that the primary mode of failure in compression is tensile rather than shear (eg. Senkov et al. 2011). The ductility in moderately ductile HEAs is slip dominated and fracture is generally an outcome of the interaction between the localization of deformation (normally expressed in the form of shear bands) and grain boundaries. The ductility on the macroscopic scale is thus related to mode I loading.

Based on the above postulate, we investigate the intrinsic ductility and fracture of these HEAs within the Linear Elastic Fracture Mechanics (LEFM) framework. The analysis takes into consideration dislocation emission only and neglects twinning due to experimental evidence suggesting that it can be neglected (Ohr, 1985). Bcc metals are also known for not exhibiting stable stacking faults that would enable twinning mechanisms. A ductility index D is hence defined as follows :

$$D = K_{Ie} / K_{Ic} \quad (x)$$

Where,

If $D < 1$, the material will be ductile

If $D \geq 1$, the material will be brittle

Theory :

The LEFM solutions assume plane-strain condition (i.e. $e_{zz} = 0$) and small deformation.

The critical stress intensity factor for cleavage is given by Griffith condition[23] :

$$K_{Ic} = (2.\gamma_{SURF} / \Lambda_{22})^{0.5} \quad (xi)$$

Where,

γ_{SURF} = Energy of formation of free surface

Λ_{22} = Anisotropic elasticity parameter (Appendix A)

The critical stress intensity factor for emission is given by using Rice model[24] :

$$K_{Ie} = (G_{Ie} . o(\varphi,\theta))^{0.5} / F_{12}(\theta) . \cos(\theta) \quad (xii)$$

Where,

G_{Ie} = Critical energy release rate for dislocation emission.

$o(\varphi,\theta)$, $F_{12}(\theta)$ = Anisotropic elastic parameters (Appendix A)

The G_{Ie} is equated to the Unstable Stacking Fault energy (γ_{USF})for

the bcc metals and the ductility index D is hence reduced to :

$D = \chi\gamma$, (xiii)

Where,

$\chi = (\Lambda_{22} . o(\varphi,\theta))^{0.5} / (\sqrt{2} . \cos(\theta) . F_{12}(\theta))$

$\gamma = (\gamma_{USF} / \gamma_{SURF})$

2. LLD metric[7] :

Bcc refractory HEAs are known to possess a weak yield-strength dependence on Temperature and a sharp brittle to ductile transition with increasing temperature. The strengthening mechanisms of these refractory metals and alloys have been a subject of research for a long time now. One of the more widely accepted mechanisms is the solid-solution strengthening that is attributed to the local lattice distortions in the crystal structures. For HEAs, this is accompanied by the high degree of mismatch between the atomic sizes and the large variation in the elastic modulus within the crystal that are known to impede dislocation motion [25].

It is hypothesized that the ductility in bcc refractory HEAs can be attributed to the quantum-mechanical phenomena like the distortion of the crystal lattice in the local chemical environment and the chemical disorder during the formation of these alloys. This will increase the electronic band dispersion and cause disorder broadening. Local lattice distortions which are caused due to the mismatch in atomic sizes and elastic modulii result in the formation

of multiple new dislocation pathways. There is also a correlation between the electronegativity differences due to the complex chemical environments and the change in the energies for vacancy formation as well as the migration barriers within these HEA crystals. Local lattice distortions also result in localized strains in the crystal structure and impede dislocation motion.

This framework attempts to use the correlation between the local lattice distortions and the Valence Electron Concentration (VEC) for predicting the ductility of bcc refractory HEAs. A dimensionless parameter of quantum-mechanical origin called LLD was defined as follows :

$$LLD = \Delta w_{VEC} \times \Delta u_{x,y,z} / [(\Delta u_{x,y,z})^2]^{0.5} \quad \text{(xiv)}$$

Where,

If LLD < 0.3, the material will be ductile

If LLD $\geq$ 0.3, the material will be brittle

The parameter $\Delta u_{x,y,z}$ is the average atomic displacement and $[(\Delta u_{x,y,z})^2]^{0.5}$ is the $L_{2,1}$ norm of the atomic displacements calculated by minimizing the Hellman-Feynman forces for a perfect crystal supercell. Δw_{VEC} is the weighted average of the VEC for the specific HEA. The initial perfect lattice coordinates before relaxing the bulk structures are taken as the initial positions and the positions of atoms in the ground state energies relaxed using DFT are taken as the final atomic positions {3.1}. The distance moved by each atom is averaged out to calculate $\Delta u_{x,y,z}$ and the $L_{1,2}$ norm of these distances is calculated to find the $[(\Delta u_{x,y,z})^2]^{0.5}$.

The Δw_{VEC} is the weighted Valence electron concentration and is calculated by taking the difference between the VEC of the HEA that is studied and (VEC_{max} -VEC_{min}). For bcc alloys, (VEC_{max} -VEC_{min}) is the difference between the phase formation range , i.e. (6-4) = 2. This component of the equation ensures that the electronegativity is taken into account and it offsets the superficial dominance of the atomic displacements.

3. Surrogate ductility index D[8] :

There are several well established ideas to tackle the problem of ductility prediction in cc HEAs. One of the most widely accepted criteria is based on the Rice criterion based on the failure by fracture determined by the competition between the rate of dislocation emission vs the rate of crack propagation for an atomistically sharp crack[6,7]. This model is an approximation of the Rice model but is relatively much more efficient.

This new parameter was defined to predict the approximate ductility while retaining the basic idea of the Rice model that the competition between the dislocation emission and the crack propagation can be approximated by the energies required to form new surfaces vs dislocation motion at the crack tip. This approximate ductility metric is called the ductility index D is defined as :

$$D = \gamma_{Surf} / \gamma_{USF} \quad \text{(xv)}$$

Where,

As the value of D increases, the alloy is more likely to be intrinsically ductile.

This approximate D parameter has a much lower computational expense as compared to the Rice criterion as it does not require the calculation of the elastic constants and only needs the free surface and unstable stacking fault energies. The accuracy of these datasets can be improved by using statistical models to use physics-informed descriptors alongside the approximate D parameter. Either way, this approximate D parameter can be a computationally effective method for forming ductility prediction models in many cases.

4. Pugh's ratio[10][11][12] :

The Pugh's ratio is the most widely used ductility criteria for metals, mostly due to how old and well established it is as well as the ease of use as it needs just the stiffness matrix for the ductility prediction. It is defined as :

$$\text{Pugh ratio} = G / K , \qquad \text{(xvi)}$$

Where,

G is the shear modulus of the material,

K is the bulk modulus of the material.

The Pugh ratio is an empirical model based on the competition between plasticity and fracture. If plasticity is easier to occur, the metal would be ductile and if fracture is easier, the material would be brittle. Yield strength was assumed to be a parameter to measure

the plasticity deformation. This yield strength is dependent on the shear modulus using the Orowan Bowing equation[10] :

$$\sigma_y = G \cdot b / \boldsymbol{\lambda} , \qquad \text{(xvii)}$$

Where,

σ_y is the yield stress,

G is the shear modulus,

b is the Burger's vector,

$\boldsymbol{\lambda}$ is the size of the Frank-Read source.

Pugh associated this with the Brinell Hardness Number (B.H.N) :

$$B.H.N = G \cdot b / c, \qquad \text{(xviii)}$$

Where,

G is the shear modulus,

b is the Burger's vector,

c is a constant for a particular crystal, not explicitly defined.

The fracture stress, on the other hand, can be related to the elastic constants as well. It was noted that the fracture stress is proportional to the Young's modulus, E. It was also noted that the surface energy where a part of the fracture work gets converted, also scales with E.

Pugh concluded that due to the constraints on the strain state at the crack tip would cause the elastic onstants to switch between two limiting cases, namely the Young's modulus E and bulk modulus K. Since both are related to the same 3 lastic constants, and by

extension scale together, bulk modulus was selected for convenience. The fracture stress hence obeys :

$$\sigma_* \propto K \cdot a, \quad \text{(xix)}$$

Where,

σ_* is the fracture stress,

K is the bulk modulus,

a is the lattice parameter.

Using the equations defined above for the B.H.N and σ_* , we get :

$$B.H.N / \sigma_* \propto G \cdot b / c \cdot K \cdot a$$

This formalism does not account for the thermal effects as well as the effects of crystal imperfections. Also, assuming that the effects of the crystal structure are neglected, i.e, b / a.c is assumed to be constant, we get the relation :

$$B.H.N / \sigma_* \propto G / K \quad \text{(xx)}$$

We defined the shear modulus as the Voigt shear modulus and is given as[12] :

$$G = (3 * C_{44} + C_{11} - C_{12}) / 5 \quad \text{(xxi)}$$

And we defined the bulk modulus as[12] :

$$K = (2 * C_{11} + C_{12}) / 3 \quad \text{(xxii)}$$

It can hence be concluded that the left hand side of the equation will have a higher value if the material is softer (hence more ductile) or if the fracture stresses are very high (less tendency to fracture) and hence it can be concluded that a material with a lower value of the right hand side of the equation, i.e, the G/K will be more likely to be ductile. Pugh did not propose a critical value of G/K for the ductile to brittle transition of metals, but further investigation suggested the value to be around 0.57 to 0.6[12].

5. Pettifor's Criteria / Cauchy Pressure for predicting ductility[12][13] :

Cauchy pressure, also known as Pettifor's criteria, is a ductility criteria proposed for materials based on the independent elastic constants C_{12} and C_{44}. It is used to describe the nature of bonding in a material. A material with directional bonding and hence a higher resistance to bond bending such as covalent solids will have negative Cauchy Pressure, i.e. $C_{44} > C_{12}$. In contrast, materials with non-directional bonding and hence a lower resistance to bond bending like metals will have a positive Cauchy Pressure. Since metals are in general more ductile than non-metals, this criterion can be used as a ductility metric defined as :

$$C'' = C_{12} - C_{44} \quad \text{(xxiii)}$$

Where,

If $C'' > 0$, bonding is likely to be metallic and ductile

If C” < 0 , bonding is likely to be covalent and less ductile.

This formalism is based on the Quantum Mechanical analysis of bond hybridization in intermetallics that the ductility of metallic alloys can be predicted based on just two individual elastic constants in a single crystal. It is derived using many body potentials that explicitly include the angular character of the bonding orbitals.[11, 12]

6. Valence Electron Concentration (VEC) :

Bcc refractory metals are transition metals from groups V and VI of the periodic table. These usually have a characteristic property of having half-filled d-band electrons. These electrons generate strong interatomic forces that create a considerable direction dependence[8]. This gives these bcc metallic alloys very high melting temperatures and substantial activation barriers for the dislocations resulting in a weaker temperature dependent strength correlation. This makes them ideal for high temperature applications where strength retention is required. However, this comes at the cost of being brittle at room temperatures due to the direction dependent behavior seen in the metallic bonds due to the strong interatomic forces between the half-filled d-band electrons. Hence, the ductility is likely to have a strong correlation with these valence electrons of these alloys.

Even though first principle DFT frameworks are widely accepted as being the most reliable, the Valence Electron Concentration (VEC) is

a quick and computationally inexpensive method to screen the potentially ductile alloys. Research in the area of bcc HEAs using electron theory has further confirmed the hypothesis that reduction of VEC for these alloys improves their ductility[26] . Hence we define a term VEC which is the Valence Electron Concentration and is the weighted average of the valence electrons in the outer s and d shells of the alloys as :

VEC = weighted average of the outermost s and d shell valence electrons of the alloys,
If VEC has a low value, the material is likely to be ductile,
If VEC has a high value, the material is likely to be less ductile.

Chapter 3

Results

3.1 Ductility predictions

3.1.1 Ductility parameter using Rice model assuming isotropic conditions in the {110} fracture plane and the 1/2 <111>{112} slip system was calculated. This slip system was chosen as it is known to be one of the two most active slip systems in bcc crystals along with the 1/2 <111>{110} slip system. Also, {110} crack plane was chosen as it along with the {100} are the typically favored cleavage planes in bcc crystals. For the 110/112 system that we have considered, the value of the parameter χ is calculated to be 1.95 for isotropic materials.[6] A total of 33 different alloys with different compositions were studied.

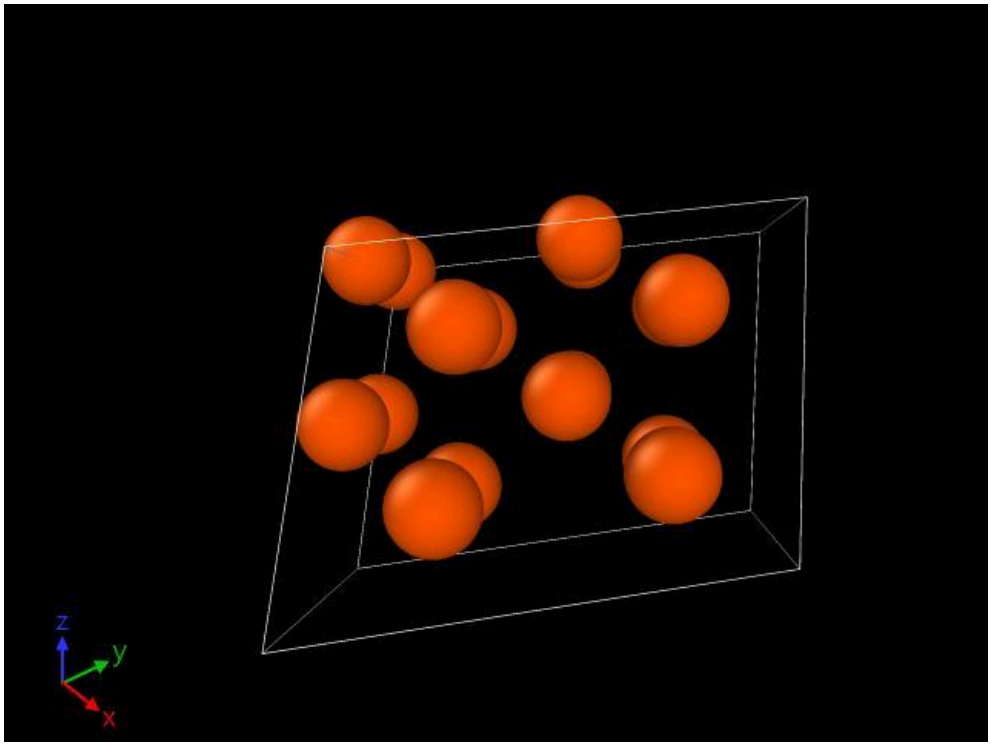

Figure 3.1.1 A figure showing a bcc supercell oriented in the orthogonal axis system oriented such that the x, y and z axis are directed in the [1 1 1] [-1 -1 2] [1 -1 0] directions respectively. This is done to simplify the computational procedure to analyze the Rice model for the [110] slip plane and [112] fracture plane. Figure generated using OVITO[33]

The ductility parameter plot as a function of the concentration of W, Ta, Cr and V is given :

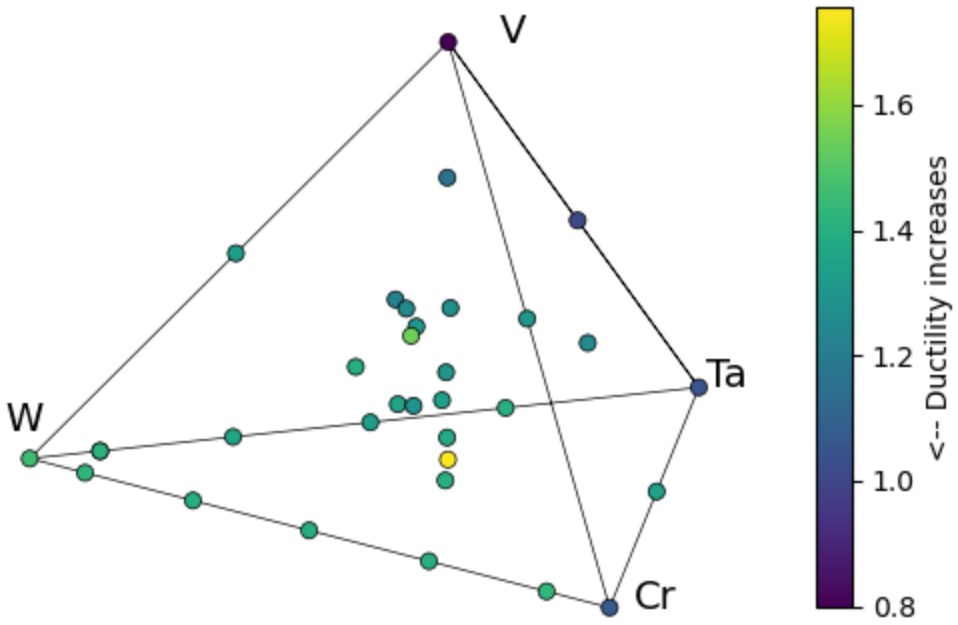

Figure 3.1.2 A tetrahedron plotting the ductility determined by the Rice model with the alloying elements as a decimal representation of the alloying elements W, Ta, Cr and V. The 4 vertices represent the points of pure elemental concentrations and go from 100% to 0% as we move from one point on any edge to the other. The edges represent binaries, the faces represent ternaries and the points inside the tetrahedron represent quarternaries. The scale represents the degree of ductility and as the color gets darker, the alloy is more ductile and as it gets lighter they get more brittle.

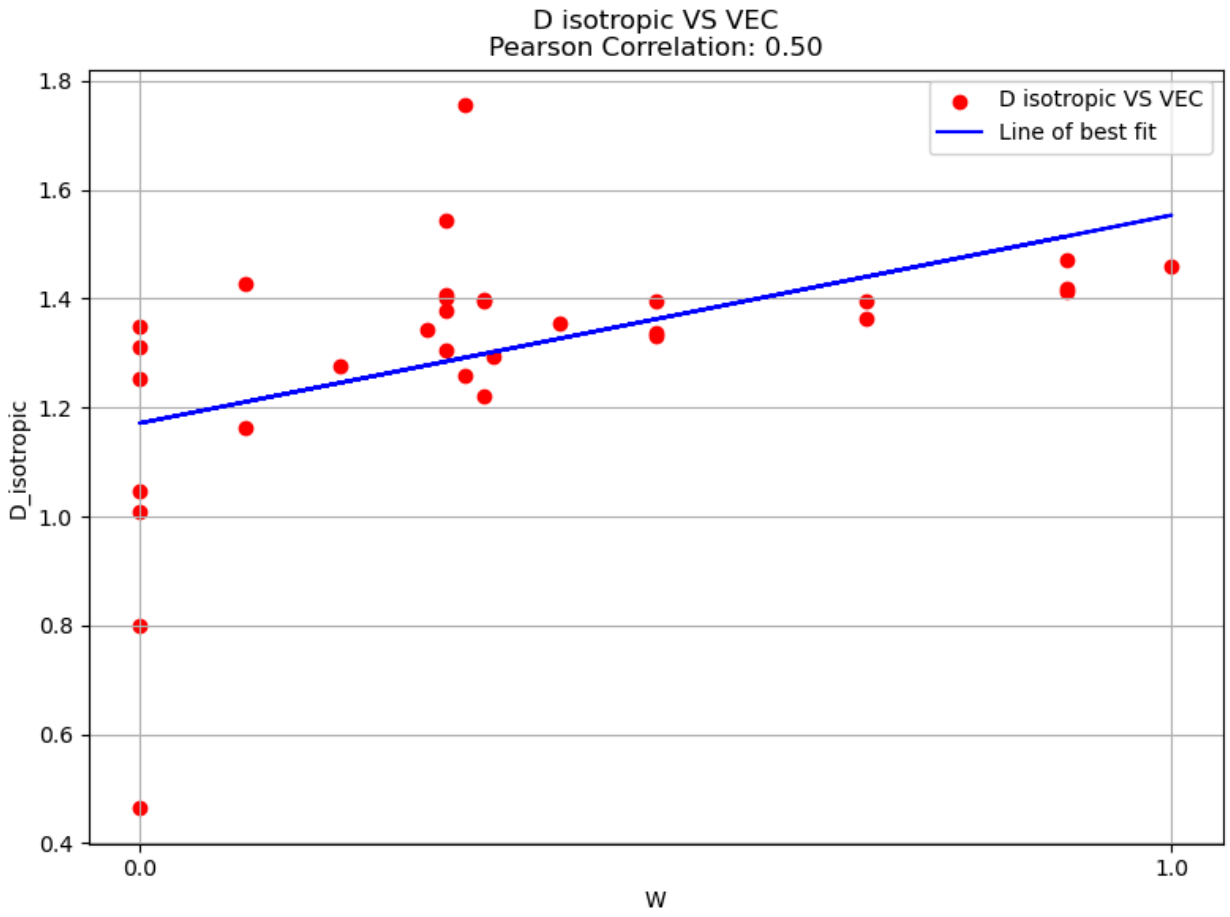

Figure 3.1.3 Pearson correlation between the concentration of W with the ductility predicted using the Rice model.

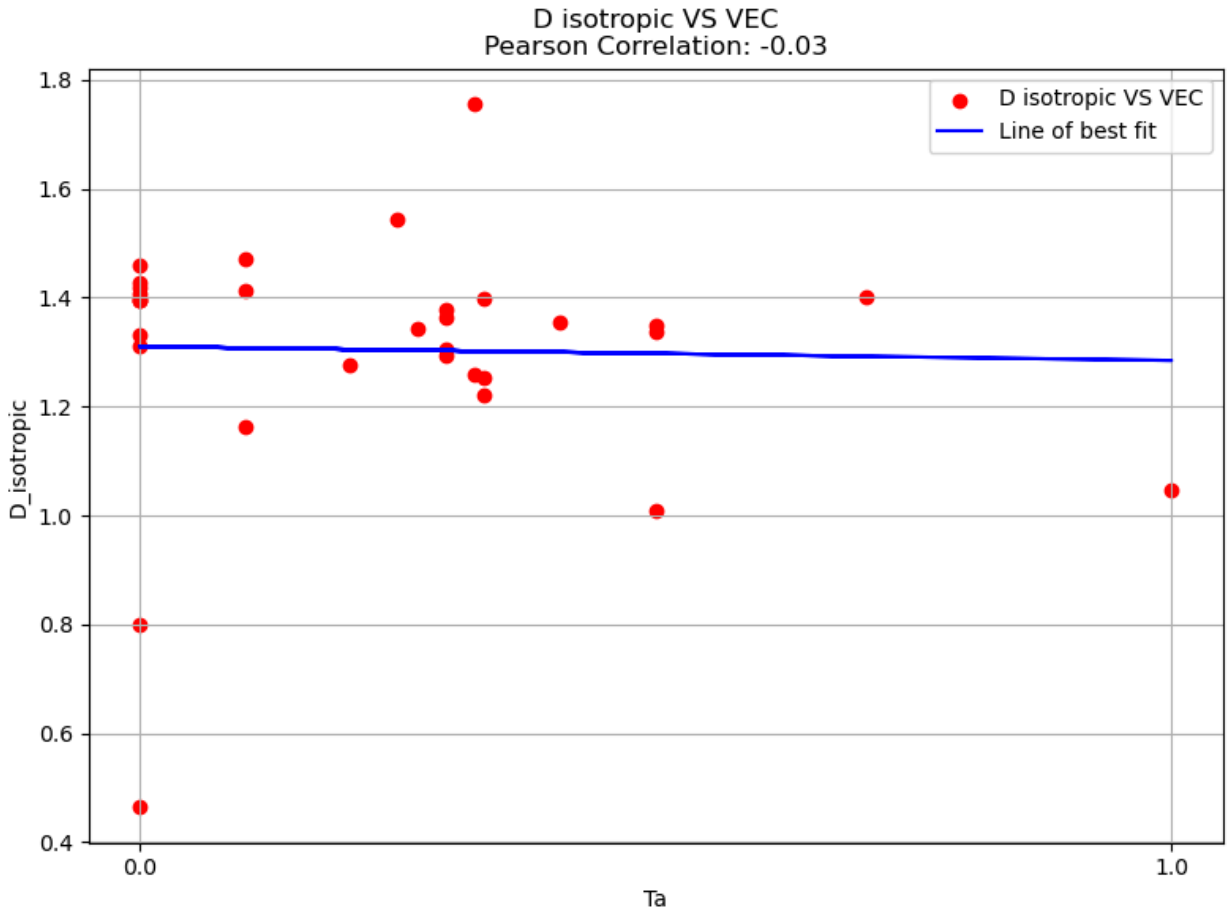

Figure 3.1.4 Pearson correlation between the concentration of Ta with the ductility predicted using the Rice model.

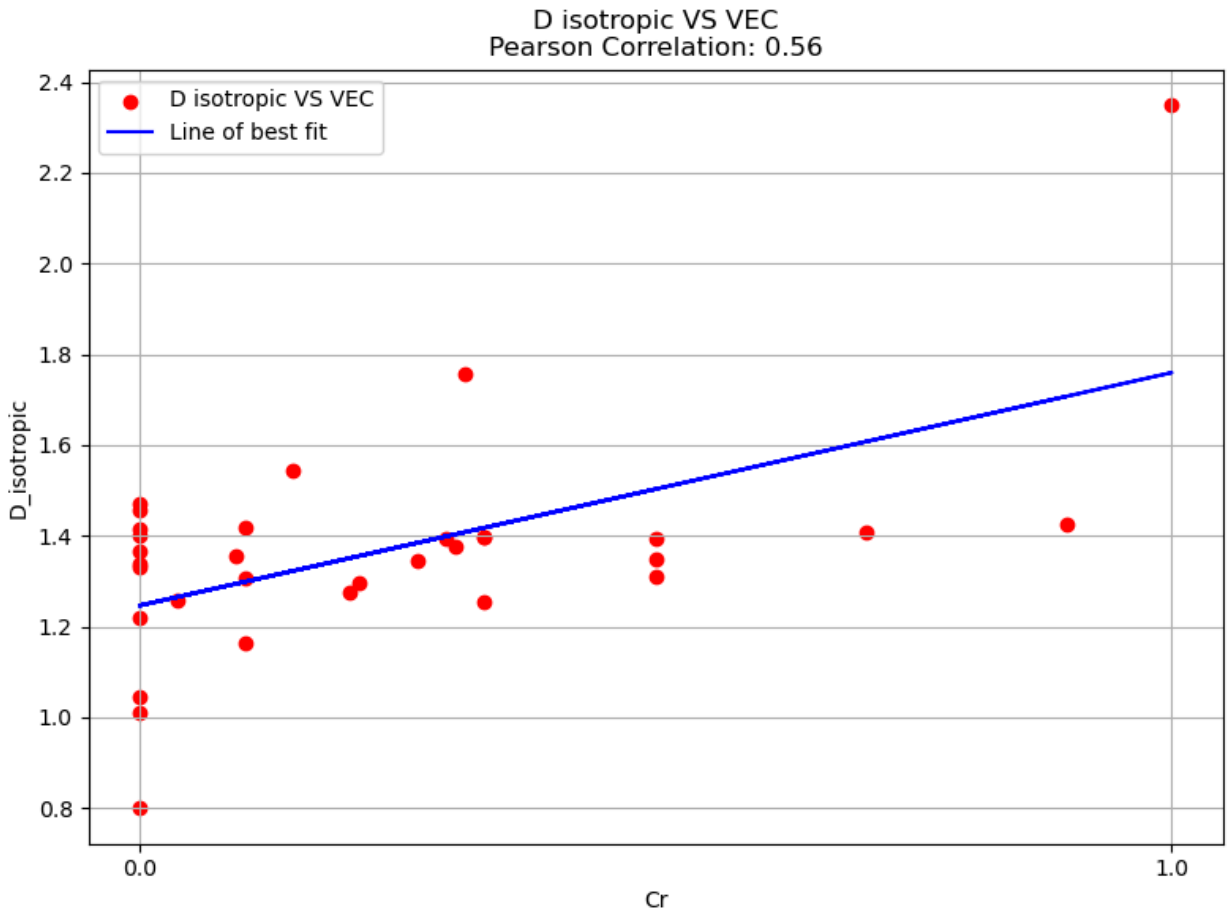

Figure 3.1.5 Pearson correlation between the concentration of Cr with the ductility predicted using the Rice model.

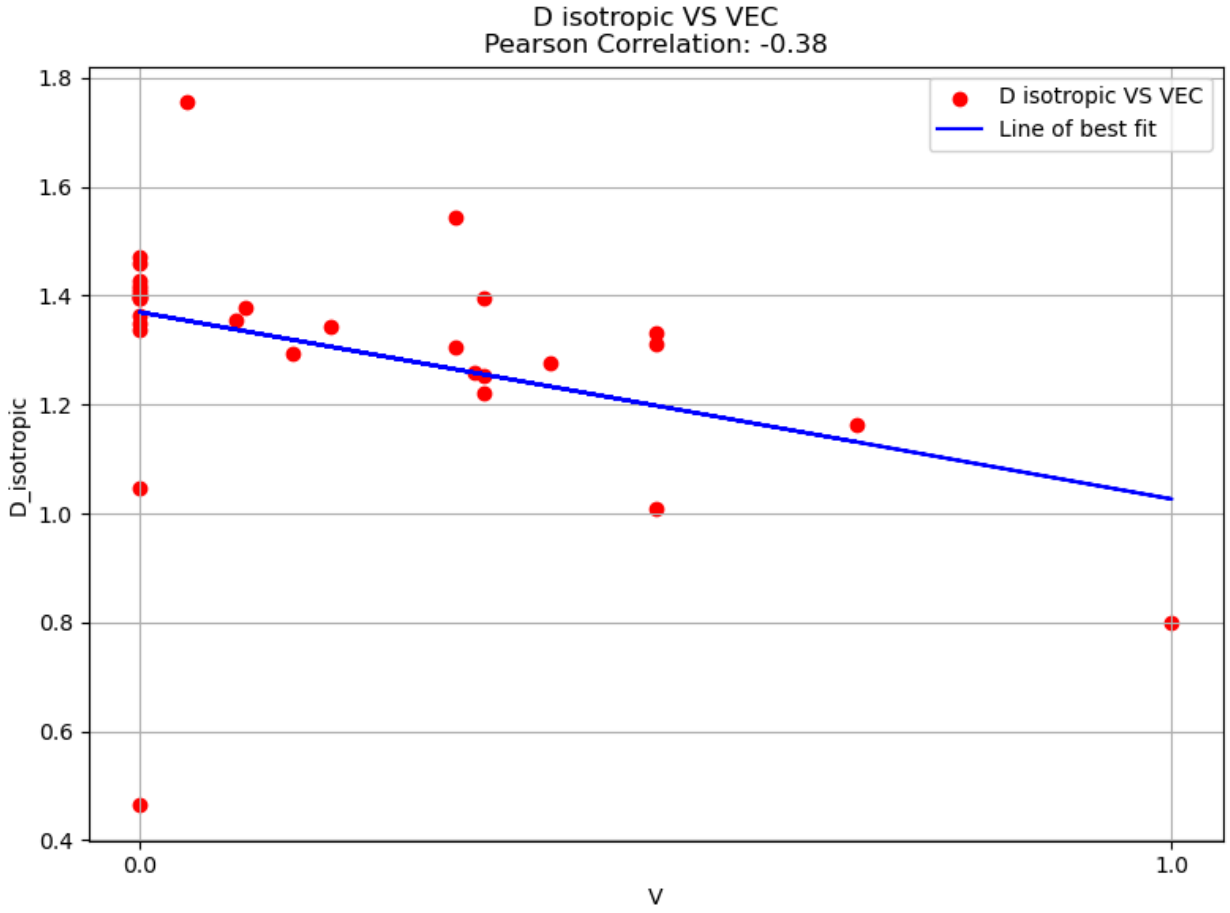

Figure 3.1.6 Pearson correlation between the concentration of V with the ductility predicted using the Rice model.

As represented by figure 3.1.1, the ductility predictions for pure elements are in good acceptance with experimental data. Pure elements V and Ta are predicted to be ductile as observed experimentally as well. W and Cr are predicted to be brittle which is also true experimentally.

The Pearson correlation plots in figures 3.1.2, 3.1.3, 3.1.4 and 3.1.5 show that there is a good correlation between the concentration of V in the alloy and the ductility. Increasing the V concentration is likely to increase the ductility of these alloys. On the other hand, W and Cr concentrations seem to have a negative

correlation with the ductility as increasing their concentrations makes the alloy more brittle. Ta concentration is seen to have a weak effect on the ductility of these alloys but it does slightly improve ductility.

Composition	W	Ta	Cr	V	Total	D isotropic	Degree of anisotropy a
1	27	27	27	27	108	1.310	1.21
2	37	32	23	16	108	1.294	1.37
3	32	27	16	33	108	1.544	1.43
4	34	35	4	35	108	1.258	1.63
5	34	35	34	5	108	1.756	1.08
6	32	32	33	11	108	1.378	1.07
7	32	32	11	33	108	1.305	1.57
8	30	29	29	20	108	1.343	1.10
9	21	22	22	43	108	1.275	1.56
10	11	11	11	75	108	1.164	1.42
11	36	36	36	0	108	1.397	1.11
12	36	36	0	36	108	1.220	1.80
13	0	108	0	0	108	1.046	1.10
14	0	0	108	0	108	1.35	0.53
15	0	0	0	108	108	0.799	1.15
16	88	88	20	20	216	1.355	1.16
17	216	0	0	0	216	1.458	1.15
18	54	54	0	0	108	1.336	1.13
19	54	0	54	0	108	1.395	0.95
20	54	0	0	54	108	1.332	0.89
21	0	54	54	0	108	1.349	1.02
22	0	54	0	54	108	1.008	0.82
23	0	0	54	54	108	1.310	0.33
24	0	36	36	36	108	1.253	1.16
25	36	0	36	36	108	1.396	1.20
26	76	32	0	0	108	1.364	1.01
27	97	11	0	0	108	1.414	0.50
28	76	0	32	0	108	1.395	0.97
29	97	0	11	0	108	1.419	0.99
30	32	0	76	0	108	1.407	
31	11	0	97	0	108	1.426	0.98
32	32	76	0	0	108	1.402	1.01
33	97	11	0	0	108	1.470	0.90

Table 3.1.1 Summary of the concentrations of the alloys alongside the degrees of anisotropies and the ductility parameter D for the system 110/112 where 110 represents the fracture plane and 112 represents the slip plane.

3.1.2 Ductility parameter using the surrogate ductility index {section 2.2.3} as a function of the concentration of W, Ta, Cr and V was calculated for 33 individual alloys. The calculations were carried out for the system 110/112 which represent the fracture and slip planes respectively.

The ductility parameter plot as a function of the concentration of W, Ta, Cr and V is given :

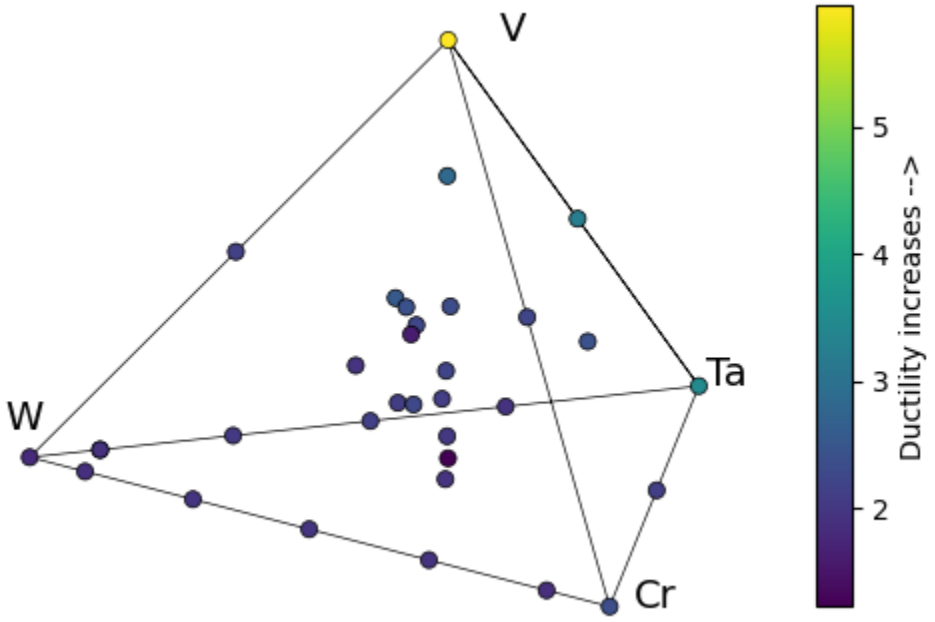

Figure 3.1.7 A tetrahedron plotting the ductility determined by the surrogate ductility index {section 2.2.3} with the alloying elements as a decimal representation of the alloying elements W, Ta, Cr and V. The 4 vertices represent the points of pure elemental concentrations and go from 100% to 0% as we move from one point on any edge to the other. The edges represent binaries, the faces represent ternaries and the points inside the tetrahedron represent quarternaries. The scale represents the degree of ductility and as the color gets lighter, the alloy is more ductile and as it gets darker they get more brittle.

As represented by the plot, the ductility predictions for pure elements are in good acceptance with experimental data. Pure elemental V is predicted to be ductile as observed experimentally as well. W is also predicted to be brittle which is also true experimentally.

The model predicts that higher concentrations of V and Ta are likely to be more ductile. There is no direct correlation between the ductility and the varying concentration of Cr, indicating that the ductility might not be greatly affected by the concentration of Cr in the alloy.

Composition	W	Ta	Cr	V	Total	Approximate
1	27	27	27	27	108	2.19
2	37	32	23	16	108	2.26
3	32	27	16	33	108	1.59
4	34	35	4	35	108	2.40
5	34	35	34	5	108	1.23
6	32	32	33	11	108	2.00
7	32	32	11	33	108	2.22
8	30	29	29	20	108	2.08
9	21	22	22	43	108	2.33
10	11	11	11	75	108	2.80
11	36	36	36	0	108	1.94
12	36	36	0	36	108	2.54
13	0	108	0	0	108	3.47
14	0	0	108	0	108	2.35
15	0	0	0	108	108	5.95
16	88	88	20	20	216	2.07
17	216	0	0	0	216	1.78
18	54	54	0	0	108	2.12
19	54	0	54	0	108	1.95
20	54	0	0	54	108	2.14
21	0	54	54	0	108	2.08
22	0	54	0	54	108	3.21
23	0	0	54	54	108	2.21
24	0	36	36	36	108	2.42
25	36	0	36	36	108	1.95
26	76	32	0	0	108	2.04
27	97	11	0	0	108	1.89
28	76	0	32	0	108	1.95
29	97	0	11	0	108	1.88
30	32	0	76	0	108	1.91
31	11	0	97	0	108	1.86
32	32	76	0	0	108	1.93
33	97	11	0	0	108	1.75

Table 3.1.2 Summary of the concentrations of the alloys alongside the degrees of anisotropies and the ductility parameter D for the system 110/112 where 110 represents the fracture plane and 112 represents the slip plane.

3.1.3 Ductility prediction using the LLD criteria {section 2.2.2} as a function of the concentration of W, Ta, Cr and V was made for 33 individual alloys.

The ductility parameter plot as a function of the concentration of W, Ta, Cr and V is given :

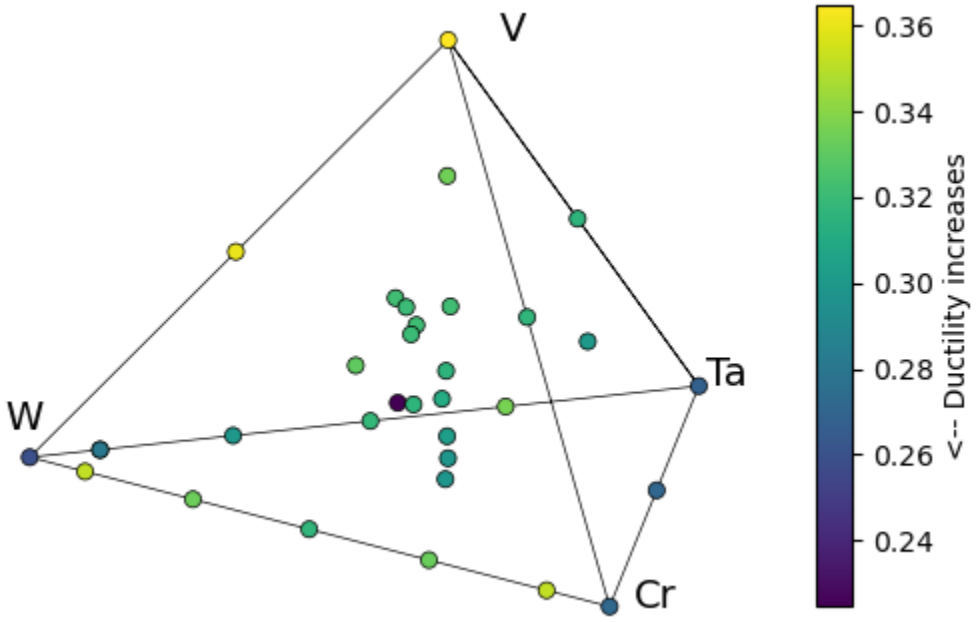

Figure 3.1.8 A tetrahedron plotting the ductility determined by the LLD ductility criteria {section 2.2.2} with the alloying elements as a decimal representation of the alloying elements W, Ta, Cr and V. The 4 vertices represent the points of pure elemental concentrations and go from 100% to 0% as we move from one point on any edge to the other. The edges represent binaries, the faces represent ternaries and the points inside the tetrahedron represent quarternaries. The scale represents the degree of ductility and as the color gets darker, the alloy is more ductile and as it gets lighter they get more brittle.

As represented by the plot, the ductilities predicted for pure elements disagree with the experimental data for pure elements, for instance, W is predicted to be ductile and V is predicted to be brittle. Although no specific trends are observed, higher concentrations of W and Ta seem to sometimes slightly improve the

ductility of the alloy.

Composition	W	Ta	Cr	V	Total	Weighted VEC	del LLD	LLD
1	27	27	27	27	108	3.50	0.0901	0.31535
2	37	32	23	16	108	3.49	0.0905	0.31584
3	32	27	16	33	108	3.60	0.0889	0.32004
4	34	35	4	35	108	3.63	0.0880	0.32014
5	34	35	34	5	108	3.36	0.0888	0.29836
6	32	32	33	11	108	3.39	0.0891	0.30276
7	32	32	11	33	108	3.60	0.0892	0.32112
8	30	29	29	20	108	3.46	0.0898	0.31096
9	21	22	22	43	108	3.59	0.0896	0.32166
10	11	11	11	75	108	3.79	0.0881	0.33442
11	36	36	36	0	108	3.33	0.0895	0.29803
12	36	36	0	36	108	3.66	0.0879	0.32171
13	0	108	0	0	108	3.00	0.0891	0.26730
14	0	0	108	0	108	3.00	0.0905	0.27150
15	0	0	0	108	108	4.00	0.0912	0.36480
16	88	88	20	20	216	3.50	0.0642	0.22470
17	216	0	0	0	216	4.00	0.0647	0.25880
18	54	54	0	0	108	3.50	0.0908	0.31780
19	54	0	54	0	108	3.50	0.0904	0.31640
20	54	0	0	54	108	4.00	0.0900	0.36000
21	0	54	54	0	108	3.00	0.0902	0.27060
22	0	54	0	54	108	3.50	0.0900	0.31500
23	0	0	54	54	108	3.50	0.0904	0.31640
24	0	36	36	36	108	3.33	0.0900	0.29970
25	36	0	36	36	108	3.66	0.0903	0.33049
26	76	32	0	0	108	3.29	0.0909	0.29960
27	97	11	0	0	108	3.10	0.0905	0.28055
28	76	0	32	0	108	3.70	0.0901	0.33337
29	97	0	11	0	108	3.89	0.0902	0.35159
30	32	0	76	0	108	3.70	0.0900	0.33300
31	11	0	97	0	108	3.89	0.0901	0.35120
32	32	76	0	0	108	3.70	0.0909	0.33633
33	97	11	0	0	108	3.89	0.0891	0.34731

Table 3.1.3 Summary of the concentrations of the alloys alongside the weighted VEC, ratio $\Delta u_{x,y,z}$ /

$[(\Delta u_{x,y,z})^2]^{0.5}$ and the predicted LLD parameter. Values of LLD below 0.3 predict ductile behavior.

3.1.4 Ductility prediction using the Pugh ratio {section 2.2.4} as a function of the concentration of W, Ta, Cr and V was made for 33 individual alloys.

The ductility parameter plot as a function of the concentration of W, Ta, Cr and V is given :

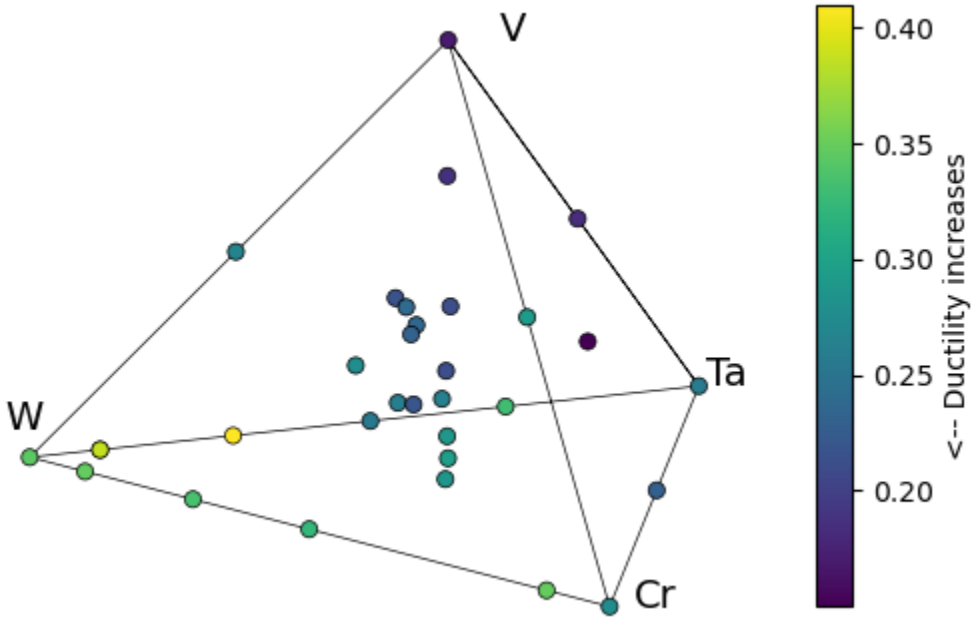

Figure 3.1.9 A tetrahedron plotting the ductility determined by the Pugh ratio {section 2.2.4} with the alloying elements as a decimal representation of the alloying elements W, Ta, Cr and V. The 4 vertices represent the points of pure elemental concentrations and go from 100% to 0% as we move from one point on any edge to the other. The edges represent binaries, the faces represent ternaries and the points inside the tetrahedron represent quarternaries. The scale represents the degree of ductility and as the color gets darker, the alloy is more ductile and as it gets lighter they get more brittle.

As represented by the plot, the ductility predictions for pure elements are in good acceptance with experimental data. Pure elemental V is predicted to be ductile as observed experimentally as well. W is also predicted to be brittle which is also true experimentally.

The model predicts that higher concentrations of V and Ta are likely to be more ductile. There is no direct correlation between the ductility and the varying concentration of Cr, indicating that the ductility might not be greatly affected by the concentration of Cr in the alloy.

Composition	W	Ta	Cr	V	Total	Shear Modulus (GPa)	Bulk Modulus (GPa)	Pugh Ratio
1	27	27	27	27	108	53.68	252.63	0.2124
2	37	32	23	16	108	57.78	263.47	0.2193
3	32	27	16	33	108	59.48	256.94	0.2314
4	34	35	4	35	108	59.57	249.59	0.2386
5	34	35	34	5	108	87.72	297.30	0.2950
6	32	32	33	11	108	83.99	291.83	0.2878
7	32	32	11	33	108	59.53	252.40	0.2358
8	30	29	29	20	108	72.65	277.55	0.2617
9	21	22	22	43	108	51.22	242.69	0.2110
10	11	11	11	75	108	41.11	221.28	0.1857
11	36	36	36	0	108	86.08	300.40	0.2865
12	36	36	0	36	108	48.82	225.21	0.2167
13	0	108	0	0	108	59.48	231.33	0.2571
14	0	0	108	0	108	86.6	314.66	0.2752
15	0	0	0	108	108	32.18	190.07	0.1693
16	88	88	20	20	216	74.20	285.71	0.2597
17	216	0	0	0	216	137.39	399.02	0.3443
18	54	54	0	0	108	75.81	297.69	0.2546
19	54	0	54	0	108	115.48	357.53	0.3229
20	54	0	0	54	108	78.61	295.50	0.2660
21	0	54	54	0	108	57.54	251.42	0.2288
22	0	54	0	54	108	39.89	218.44	0.1826
23	0	0	54	54	108	77.65	266.07	0.2918
24	0	36	36	36	108	33.57	223.63	0.1501
25	36	0	36	36	108	73.9	267.53	0.2762
26	76	32	0	0	108	101.07	246.57	0.4099
27	97	11	0	0	108	147.05	380.03	0.3869
28	76	0	32	0	108	125.32	375.42	0.3338
29	97	0	11	0	108	138.38	397.78	0.3478
30	32	0	76	0	108			
31	11	0	97	0	108	139.26	399.12	0.3489
32	32	76	0	0	108	117	354.55	0.3299
33	97	11	0	0	108	140	401.10	0.3490

Table 3.1.4 Summary of the concentrations of the alloys alongside the Shear modulus, bulk modulus and the Pugh ratio. Lower values of Pugh ratio predict ductile behavior.

3.1.5 Ductility prediction using the Cauchy Pressure {section 2.2.5} as a function of the concentration of W, Ta, Cr and V was made for 33 individual alloys.

The ductility parameter plot as a function of the concentration of W, Ta, Cr and V is given :

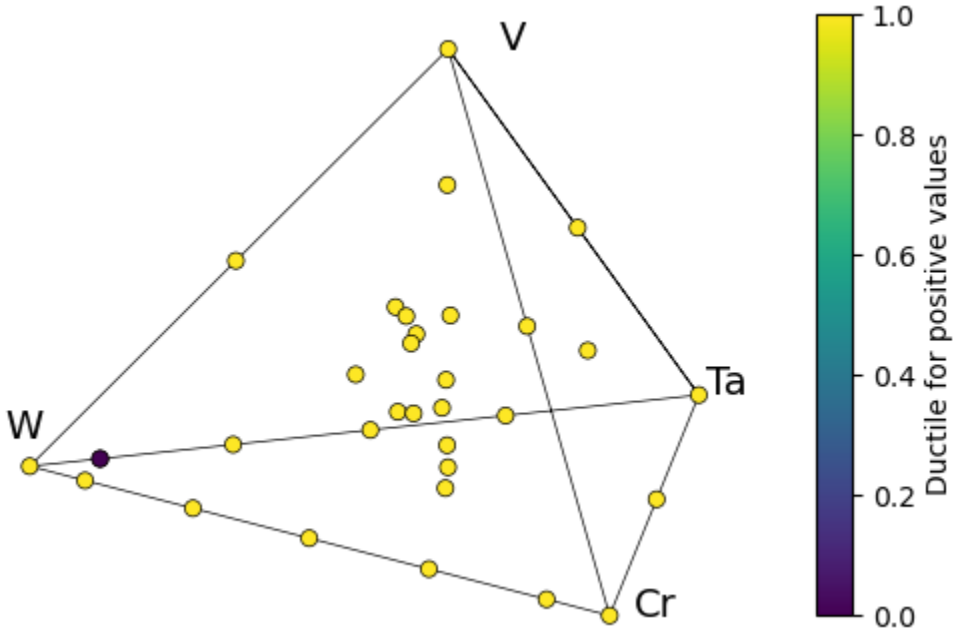

Figure 3.1.10 A tetrahedron plotting the ductility determined by the Cauchy pressure {section 2.2.5} with the alloying elements as a decimal representation of the alloying elements W, Ta, Cr and V. The 4 vertices represent the points of pure elemental concentrations and go from 100% to 0% as we move from one point on any edge to the other. The edges represent binaries, the faces represent ternaries and the points inside the tetrahedron represent quarternaries. The scale represents the degree of ductility and as the color gets darker, the alloy is more ductile and as it gets lighter they get more brittle.

The model predicts that most alloys have bonding that is more metallic and non - directional in nature resulting in ductile elements. However, one W-Ta binary is predicted to possess directional bonding and is hence predicted to be brittle. This model is not in very good acceptance with experimental data as pure W is predicted to be ductile by this model but is actually brittle.

Composition	W	Ta	Cr	V	Total	Cauchy Pressure (GPa)
1	27	27	27	27	108	+
2	37	32	23	16	108	+
3	32	27	16	33	108	+
4	34	35	4	35	108	+
5	34	35	34	5	108	+
6	32	32	33	11	108	+
7	32	32	11	33	108	+
8	30	29	29	20	108	+
9	21	22	22	43	108	+
10	11	11	11	75	108	+
11	36	36	36	0	108	+
12	36	36	0	36	108	+
13	0	108	0	0	108	+
14	0	0	108	0	108	+
15	0	0	0	108	108	+
16	88	88	20	20	216	+
17	216	0	0	0	216	+
18	54	54	0	0	108	+
19	54	0	54	0	108	+
20	54	0	0	54	108	+
21	0	54	54	0	108	+
22	0	54	0	54	108	+
23	0	0	54	54	108	+
24	0	36	36	36	108	+
25	36	0	36	36	108	+
26	76	32	0	0	108	+
27	97	11	0	0	108	-
28	76	0	32	0	108	+
29	97	0	11	0	108	+
30	32	0	76	0	108	+
31	11	0	97	0	108	+
32	32	76	0	0	108	+
33	97	11	0	0	108	+

Table 3.1.5 Summary of the concentrations of the alloys alongside the Cauchy pressure. Positive values of Cauchy pressure predict ductile behavior.

3.2 Screening for ductility using approximate and phenomenological models :

The Rice model is by far the only analytical and most physics informed ductility prediction model discussed in this work. However, it is also computationally most expensive due to the large number of DFT calculations involved. The extremely large compositional space of HEAs makes it practically impossible to run all the possible alloys through the Rice model as it would be extremely time consuming and computationally expensive.

One way to tackle this problem is by setting up surrogate models for screening the vast number of possible alloys to a manageable number which can then be analyzed using the Rice model. The requirements for this method to improve the computational efficiency is that these surrogate models need to be in good agreement with the Rice model and they should be less expensive computationally. Five ductility models are discussed in this work which are either an approximation of the Rice model or are phenomenological in nature. This makes them inherently less reliable and accurate. However, all of the models require a significantly lower computational time and resources than the Rice model to calculate which makes them relatively more efficient.

Following sections analyzes the viability of each framework as a surrogate model for screening :

3.2.1 Rice model vs Approximate D parameter {Section 2.2.3} :

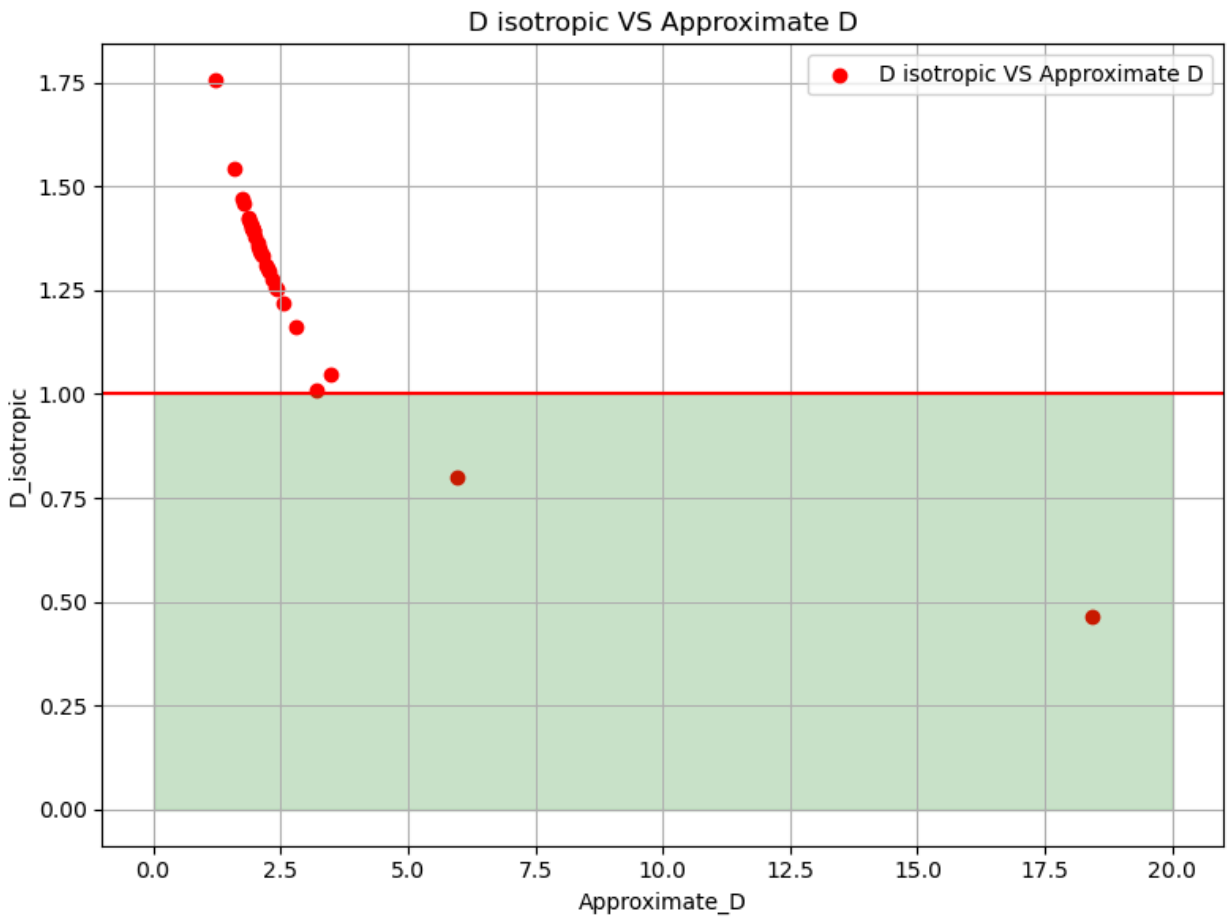

Figure 3.2.1 Correlation between the D parameter for isotropic materials using the Rice model (y-axis) vs the approximate D parameter (x-axis) using the surrogate model {Section 2.2.3}. The area shaded in green is ductile according to the Rice model on the Y-axis and the higher values of the Approximate D on X-axis predicts higher ductility.

It is evident from the plot that the surrogate model described in {section 2.2.3} is in good agreement with the Rice model. It can be concluded that this approximate formulation can be used as a surrogate model to predict the ductility from a large pool of HEAs to screen out the alloys that are more likely to be ductile. This can greatly help reduce the time and computational expense by limiting the number of alloys to be studied using the Rice model.

3.2.2 Rice model vs LLD {Section 2.2.2} :

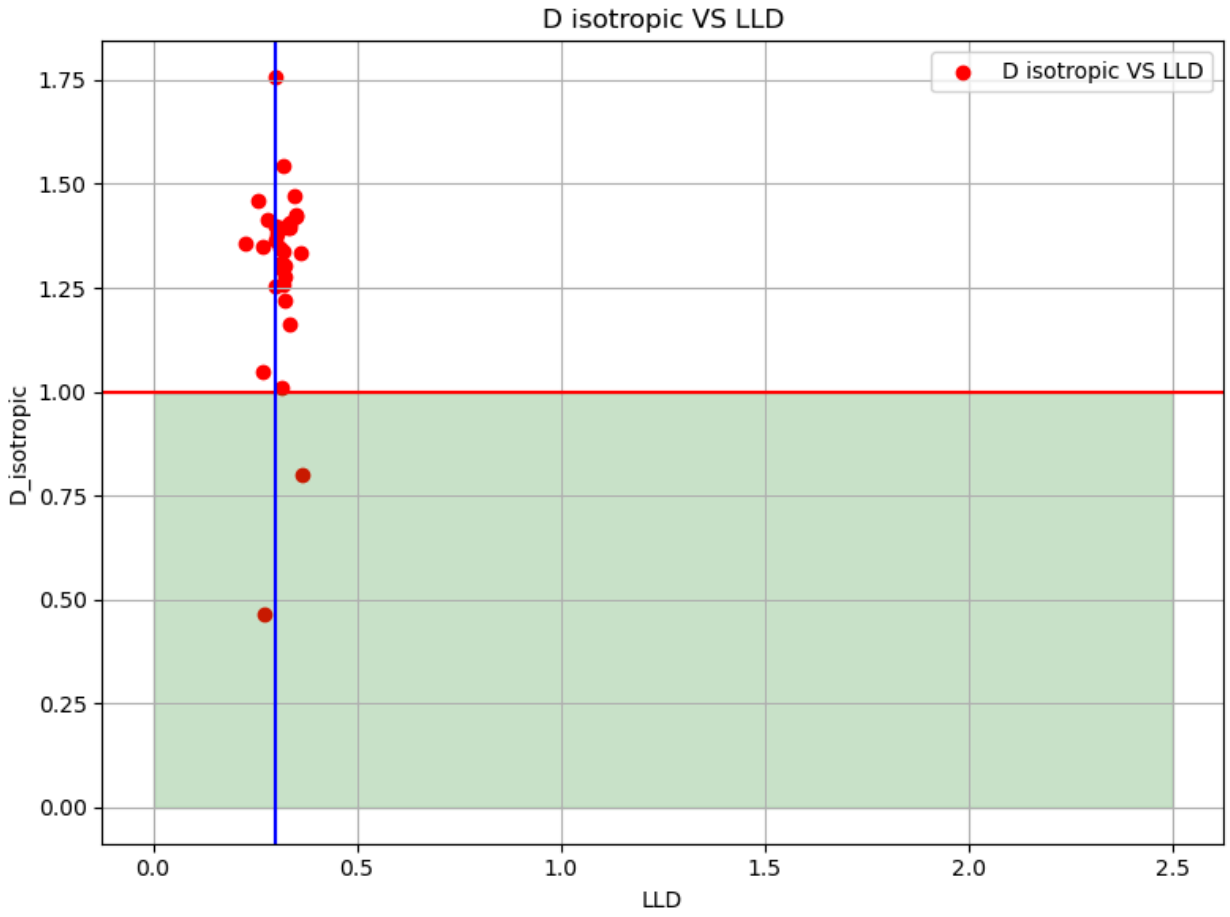

Figure 3.2.2 Correlation between the D parameter for isotropic materials using the Rice model vs the LLD parameter {Section 2.2.2}. The area shaded in green is ductile according to the Rice model on the Y-axis and the values of LLD on the X-axis with values on the left of the blue line, i.e. below 0.3 are predicted to be ductile.

It is evident from the plot that the phenomenological model described in {section 2.2.2} is not in a good agreement with the Rice model. Even though there is a correlation, the two parameters disagree for multiple alloys. Even so, the computationally inexpensive nature makes the LLD parameter much more efficient than the Rice model. It can be concluded that this formulation can be

used as a surrogate model to predict the ductility from a large pool of HEAs to screen out the alloys that are more likely to be ductile. The poor correlation however would suggest that the accuracy of the screening would not be very reliable.

3.2.3 Rice model vs Pugh ratio {Section 2.2.4} :

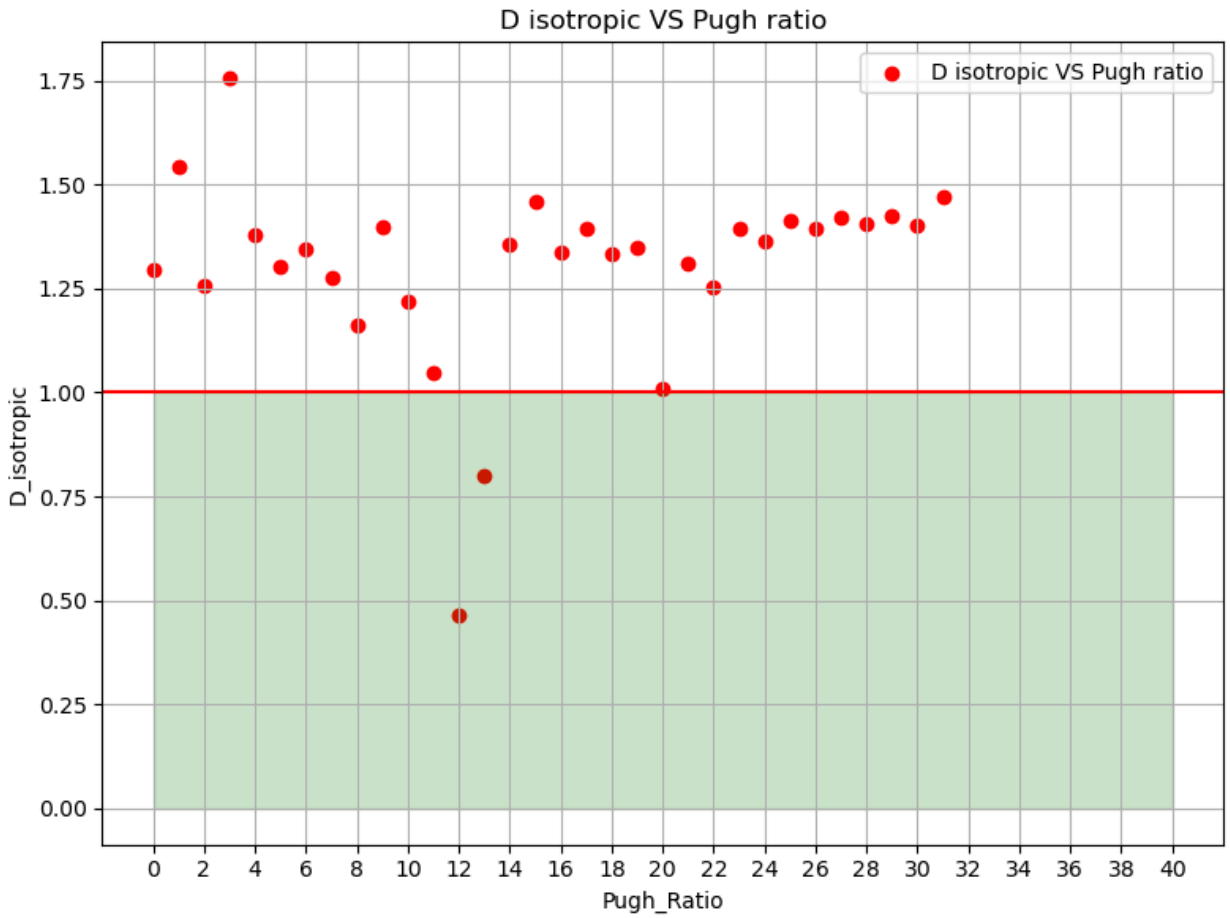

Figure 3.2.3 Correlation between the D parameter for isotropic materials using the Rice model vs the Pugh ratio {Section 2.2.4}. The area shaded in green is ductile according to the Rice model on the Y-axis and the lower values of the Pugh ratio on the X-axis predicts higher ductility.

The Pugh ratio described in {section 2.2.4} is not in a good agreement with the Rice model. It can be concluded that this formulation cannot be used as a surrogate model to predict the ductility as even if the method is computationally less expensive , the accuracy of the screening would not be very reliable.

3.2.4 Rice model vs Cauchy pressure {Section 2.2.5} :

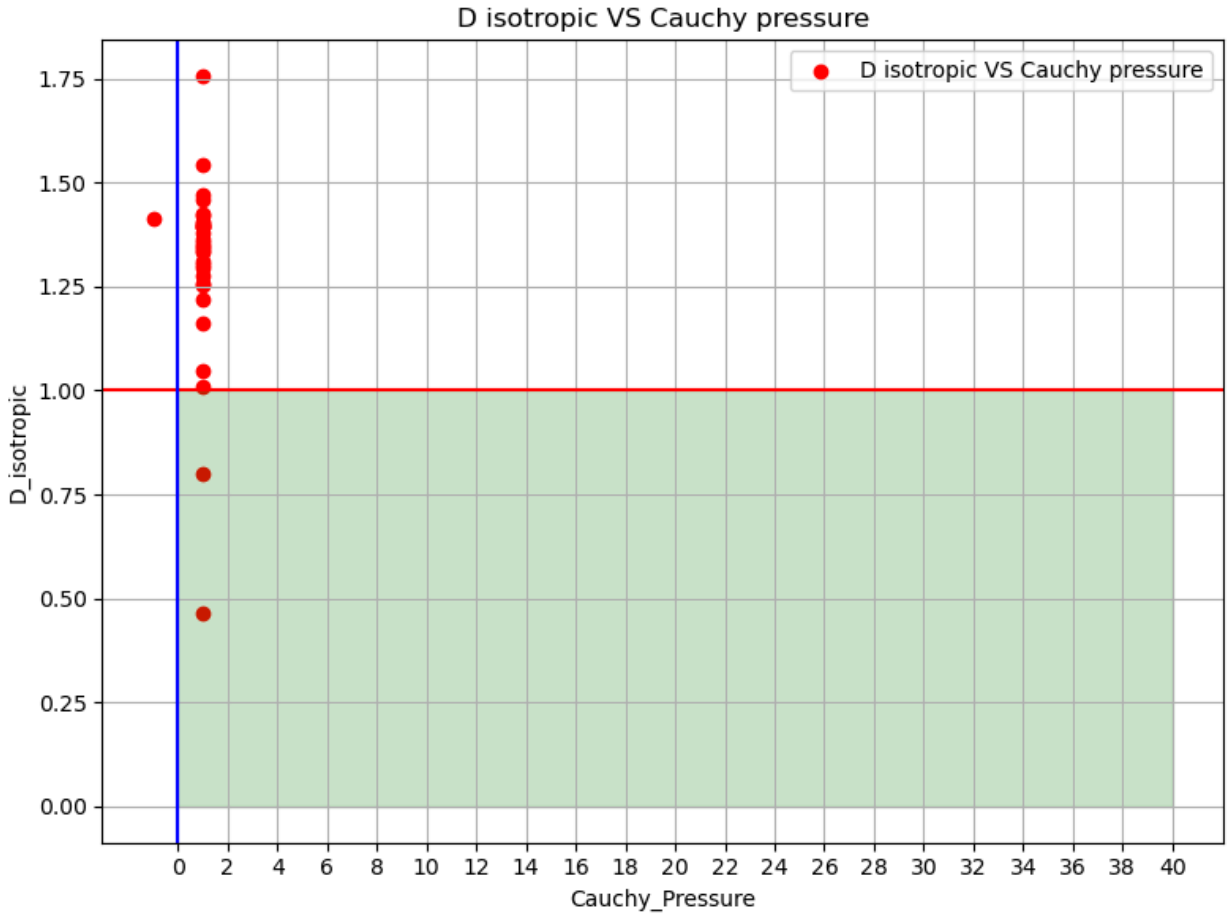

Figure 3.2.4 Correlation between the D parameter for isotropic materials using the Rice model vs the Cauchy ratio {Section 2.2.5}. The area shaded in green is ductile according to the Rice model on the Y-axis and the negative values of Cauchy pressure on the X-axis with values on the left of the blue line, i.e. below 0 are predicted to be ductile.

The Cauchy pressure described in {section 2.2.5} is not in a good agreement with the Rice model. It can be concluded that this formulation cannot be used as a surrogate model to predict the ductility as even if the method is computationally less expensive, the accuracy of the screening would not be very reliable.

3.2.5 Rice model vs VEC{Section 2.2.6} :

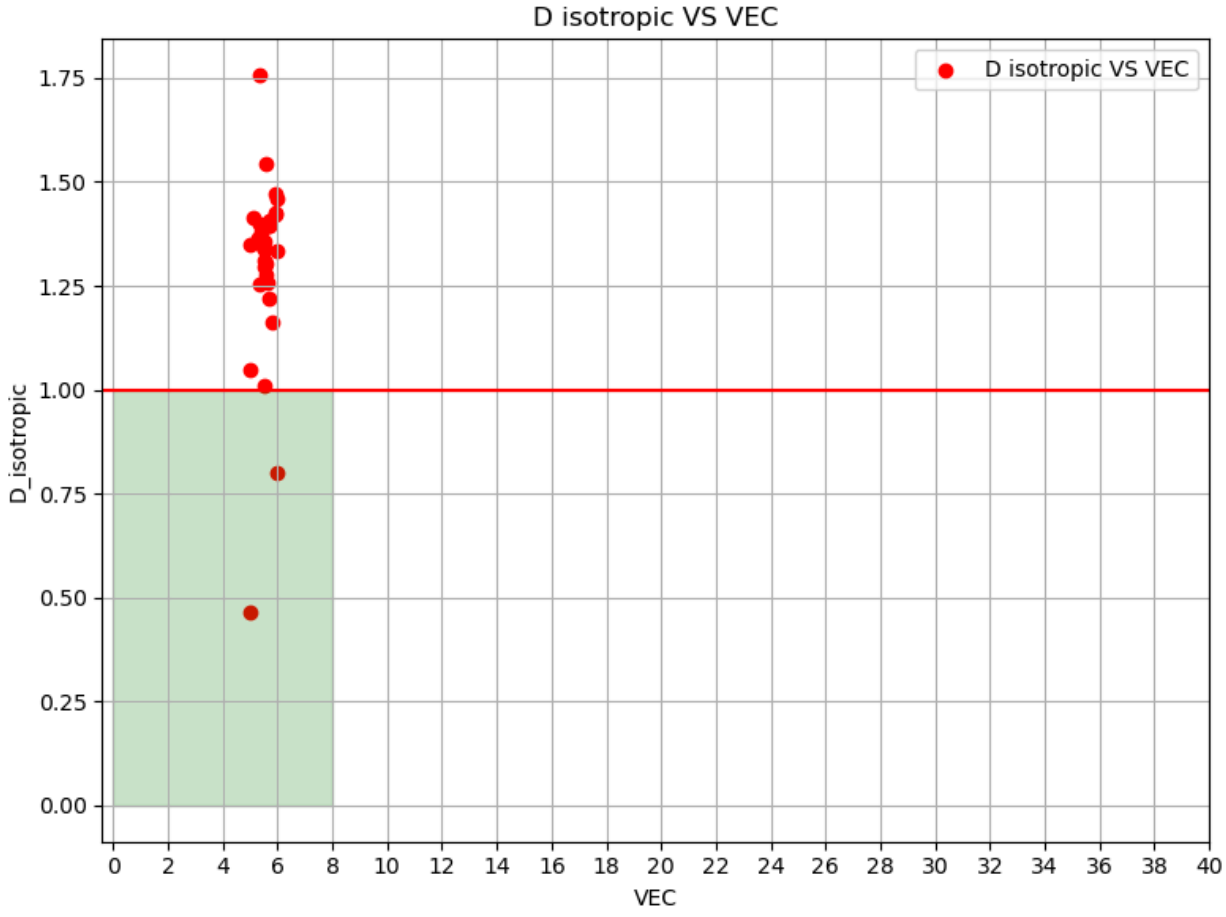

Figure 3.2.5 Correlation between the D parameter for isotropic materials using the Rice model vs the VEC {Section 2.2.6}. The area shaded in green is ductile according to the Rice model on the Y-axis and the lower VEC values on the X-axis are predicted to be ductile.

The VEC described in {section 2.2.6} is not in a good agreement with the Rice model. It can be concluded that this formulation can not be used as a surrogate model to predict the ductility as even if the method is computationally less expensive, the accuracy of the screening would not be reliable.

3.3 Cluster expansion for the prediction ground state energies :

In this work, we make use of ATAT to develop a CE model for predicting the bulk energies of the HEAs. The ATAT uses a perfect crystal lattice structure as reference and the ground state energies of a few structures along with the structures themselves for calculating the correlation functions. For every added structure, a corresponding CV score is calculated which is an indicator of the accuracy of the correlation functions. Weights can be assigned to some specific alloys during the calculations.

We make use of the datasets obtained in {section 2.2.1 and 2.1.2} to train the CE model for calculating the correlation functions. Additional weights of 3x were assigned to the pure elements as it was found to improve the accuracy. The enthalpies of mixing per unit atom[29] were computed as :

$$\Delta H_{mix}(\sigma) = E_{total}(\sigma) - (\sum^{k}_{p=1} c_p \, . \, E_{total}(p)) \qquad \text{(xxiv)}$$

Where,

$\Delta H_{mix}(\sigma)$ is the enthalpy of mixing per atom for alloy σ,

$E_{total}(\sigma)$ is the energy per atom of the alloys σ,

$E_{total}(p)$ is the total energy of pure element p,

c_p is the concentration of the pure element p in alloy σ.

The CV score obtained was 0.003 which is considered good and it can be concluded that the CE model has good levels of predictive accuracy.

Chapter 4

Limitations and future scope of the study

4.1 Rice model for anisotropic materials and for different crack systems :

The Rice model is an analytical model that makes use of the Stroh formalism for the LEFM solutions. This formalism is defined well for cubic anisotropic systems. However, due to the limited scope of this research which only studies W-Ta-Cr-V based HEAs that are mostly found to be close to isotropic systems {see table 3.1.1}, the calculations were made assuming the alloys to be isotropic. In the future, this work can be extended to study anisotropic systems as well to have a more general framework for ductility prediction.

Also, due to the 110/112 crack system being the most active, this was the only system studied. There are at least 15 other possibly active crack systems[28] out of which the 100/110 system is significant[6]. These systems need to be studied to obtain a holistic understanding of the ductility in these alloys.

4.2 Calculations for pure Cr :

The DFT methodologies used in this research seem to be inconsistent with the experimental data as well as data from other computational methods with a high error. Due to this reason, the data sets for this particular alloy containing 100 % Cr were not calculated and were taken from other works of research[20][30]. The investigation for this anomaly and developing a DFT framework that successfully gives out the correct data is an interesting problem that needs to be addressed in the future.

4.3 Cluster expansion for predicting γ_{Surf}, γ_{USF} and elastic constants :

The current research successfully predicts the ground state energies using a CE model using ATAT with high accuracies. However, the Rice model needs additional parameters to predict the ductility of these alloys which are the γ_{Surf}, γ_{USF} and elastic constants. Once we have a good CE framework for predicting all these parameters, a holistic framework to predict the ductility of any similar HEA can be developed that will greatly improve the efficiency in this research area.

4.4 Verification of ductility predictions using state of the art experimental methods

Computational models like this are a cost effective way of predicting material properties without actually manufacturing or performing experiments. But these methods are never fully perfect and we always need experimental validation for accepting the accuracy of these models as well as for verification of the predicted results. Here we discuss a state of the art experimental method for manufacturing and testing the ductility of Ti-W-Ta-Cr-V based HEAs.[38]

The fabrication procedure starts with 99.9% pure W (1.21 μm), Ti (45 μm), V (< 75 μm), Cr (63 μm) and Ta (< 45 μm) powders. These are mixed using a tubular shaker-mixer at 30 rpm for 3 hours. Steel balls in a ratio of 1:1 were added for a better mixing. The system was insulated with carbon felt-covered graphite mold to prevent heat loss. This mixture is then sintered at 1500 ^{o}C at an axial pressure of 50 MPa applied in a vacuum of 10^{-3} torr for 10 minutes.

These disc shaped samples are then subjected to room temperature compression tests on cylindrical samples with 6 mm in height and 4 mm in diameter using an Instron 5982 (Instron, USA) machine with a strain rate of 10^{-3}/s. Additionally, micro-Vickers hardness tests (402MVD, Wolpert Wilson Instruments, Germany) can be conducted for calculating the hardness of the samples. For that, the Disk-shaped sintered samples need to be cut through their cross sections for performing the tests.

This method can be used for manufacturing the W-Ta-Cr-V based HEAs studied in this research and the hardness and the fracture strains given by the room temperature compression tests can be used as measures of ductility. These results can be then compared with the computational model for studying the validation of the model as well as verification of the predicted results.

Chapter 5

Conclusion

We analyzed the analytical Rice model to calculate the ductility predictions for W-Ta-Cr-V based bcc HEAs and were successfully able to get results that seem to be in accordance with the existing computational and experimental data. The pure elements V and Ta were found to be ductile in nature whereas W and Cr were predicted to be intrinsically brittle. The concentrations of V and Ta seem to slightly improve the ductility and the concentrations of W tends to reduce the ductility of the HEAs although the correlation seems to be weak. There seems to be no correlation between the concentrations of Cr and the ductility.

Other approximate as well as phenomenological ductility prediction frameworks were also investigated to check for their viabilities as surrogate models for screening of the potentially ductile alloys before calculating the ductility using the DFT intensive Rice model. Out of all the ductility parameters studied, the D parameter {section 2.2.3} was the only parameter that shows a good correlation with the Rice model and hence has a good potential to serve as a relatively computationally inexpensive screening method for these alloys before calculating the ductility using the Rice model.

Finally, a predictive CE with good accuracy of prediction of ground states was set up to predict the ground state energies of W-Ta-Cr-V based bcc HEAs. This takes us one step closer towards formulation of a holistic prediction model for calculating the ductility of W-Ta-Cr-V based bcc HEAs.

Appendices

A.1 LEFM solution for crack propagation :

This brief summary is based on the book Anisotropic elasticity in an elastic medium[21] and related works[28]. It makes use of the Eshelby-Reid-Shockley formalism and the Stroh formalism[21] to obtain a general solution for a sharp crack tip propagation in an anisotropic, homogeneous elastic medium under uniform stress. The solutions are for a 2-dimensional plane-strain assumption.

A.1.1 Eshelby-Reid-Shockley formalism :

The stress-strain relationship is given by :

$$\boldsymbol{\sigma}_{ij} = C_{ijks} \,.\, \varepsilon_{ks} \qquad \text{(xxv)}$$

Where,

$\boldsymbol{\sigma}_{ij}$ is the stress applied on a material

C_{ijks} is the stiffness matrix of the material

ε_{ks} is the resulting strain on the material

The equation of equilibrium for a material is given by :

$$\nabla \,.\, \boldsymbol{\sigma}_{ij} + F_j = 0 \qquad \text{(xxvi)}$$

Where,

$\nabla \,.\, \boldsymbol{\sigma}_{ij}$ is the divergence of the stress on the material

F_j is the external force on the system

Assuming the stiffness matrix has all elastic symmetries,

$$C_{ijks} = C_{ksij} = C_{jiks} = C_{jisk} = C_{skji} = C_{ksji} = C_{skij} \quad \text{(xxvii)}$$

For plane-strain assumption, the solution is a linear equation in x_1 and x_2. Let z be a linear function in x_1 and x_2 such that :

$$z = x_1 + p.x_2 \quad \text{(xxviii)}$$

The displacement field is thus given by :

$$u_i = a_i \, . \, f(z) \quad \text{(xxix)}$$

Where,

u_i is the displacement field

a_i is an arbitrary vector

f(z) is an arbitrary function of z

Taking the partial derivative of u with respect to s and then j give us the following equations :

$$u_{k,s} = a_k \, . \, (\boldsymbol{\delta}_{1s} + p.\boldsymbol{\delta}_{2s}) \, f\,'(z)$$

$$u_{k,sj} = a_k \, . \, (\boldsymbol{\delta}_{1s} + p.\boldsymbol{\delta}_{2s}) \, (\boldsymbol{\delta}_{1j} + p.\boldsymbol{\delta}_{2j}) \, f\,''(z) \quad \text{(xxx)}$$

Using equation (xxiv) and (xxix),

$$\{ C_{i1k1} + p(C_{i1k2} + C_{i2k1}) + p^2(C_{i2k2}) \} \, . \, a_k = 0 \quad \text{(xxxi)}$$

From here on for simplification, we use the following notations : (xxxii)

$Q = C_{i1k1}$

$R = C_{i1k2}$

$T = C_{i2k2}$

Hence we can write equation (xxx) as follows :

$$\{ Q + p(R + R^T) + p^2T \} . a_k = 0 \qquad \text{(xxxiii)}$$

This is an eigenvalue problem. For non-trivial solution,

$$| \{ Q + p(R + R^T) + p^2T \} | = 0 \qquad \text{(xxxiv)}$$

Equation (xxxi) is a sextic equation in p. This equation will have 3 pairs of complex conjugates as roots[21]. Let p_a and a_a be the eigenvalues and eigenvectors respectively. Also, without the loss of generality, let Im p_a be positive. This shows that the roots are of the form :

$$p_{a+3} = \text{conjugate}(p_a) \qquad \text{(xxxv)}$$

$$a_{a+3} = \text{conjugate}(a_a) \qquad \text{(xxxvi)}$$

Superimposing all to form a general solution :

$$u = \sum^3_{a=1} \{ a_a . f_a(z_a) + \text{conjugate}(a_a) . f_{a+3}(\text{conjugate}(z_a)) \} \qquad \text{(xxxvii)}$$

A.1.2 Stroh formalism :

Equation (xxxviii) can be rearranged to :

$$-1/p \{ Q + p. R \} . a = \{ R^T + p . T \} = b \quad \text{(xxxviii)}$$

We now define a stress function Φ :

$$\Phi = b_i f(z) \quad \text{(xxxix)}$$

By using Hooke's law in equation (xxiv), (xxix) and (xxxvii),

$$\boldsymbol{\sigma}_{i1} = -p . b_i . f'(z) \quad \text{(xl)}$$

$$\boldsymbol{\sigma}_{i2} = b_i . f'(z) \quad \text{(xli)}$$

Using symmetry of the stress tensor, i.e. $\boldsymbol{\sigma}_{12} = \boldsymbol{\sigma}_{21}$,

$$\Phi_{1,1} + \Phi_{2,2} = 0 \quad \text{(xlii)}$$

This gives us the equation,

$$b_1 + p . b_2 = 0 \quad \text{(xliii)}$$

Writing the cumulative general solution for u and Φ,

$$u = \sum^3_{a=1} \{ a_a . f_a(z_a) \} + \{ \text{conjugate}(a_a) . f_{a+3}(\text{conjugate}(z_a)) \} \quad \text{(xliv)}$$

$$\Phi = \sum^3_{a=1} \{ b_a . f_a(z_a) \} + \{ \text{conjugate}(b_a) . f_{a+3}(\text{conjugate}(z_a)) \} \quad \text{(xlv)}$$

For most applications, f_a will have the same functional form[21]. We assume that form to be as follows, without the loss of generality :

$$f_a (z_a) = f (z_a) . q_a \quad \text{(xlvi)}$$

f_{a+3} (conjugate(z_a)) = conjugate(f (conjugate(z_a)) . conjugate(q_a) (xlvii)

Where,

q_a and conjugate(q_a) are complex conjugates.

Hence, we now have the following solutions for u and Φ.

$u = 2 . Re \{ A \langle f(z_*) \rangle \}$ (xlviii)

$\Phi = 2 . Re \{ B \langle f(z_*) \rangle \}$ (xlix)

Where,

A and B are Stroh matrices such that :

$A = [a_1\ a_2\ a_3]$ (l)

$B = [b_1\ b_2\ b_3]$ (li)

The function $\langle f(z_*) \rangle$ is given by :

$\langle f(z_*) \rangle = diag[\ f(z_1)\ f(z_2)\ f(z_3)\ ]$ (lii)

Since a and b are related by definition, for any problem, the unknowns to be determined are function $f(z_*)$ and vector q. (liii)

A.1.3 Solution for a crack tip under uniform loading in a 2-D anisotropic homogeneous elastic medium :

Using the Stroh formalism, we formulate an LEFM solution for a crack tip under uniform loading in a 2-D anisotropic homogeneous elastic medium. We assume that the uniform stress is applied at infinity and is given by $\boldsymbol{\sigma}_{ij}^{inf}$. Let the crack

length be 2a, centrally located at $x_2 = 0$, $|x_1| < a$. The crack surfaces are assumed to be traction free.

We define the stress function as follows[28] :

$\Phi = 0$, for $|x| = inf$

$\Phi = -x_1 . t_T$, for $x_2 = 0$, $|x_1| < a$

Where,

$t_T = [\boldsymbol{\sigma}^{inf}_{21}\ \boldsymbol{\sigma}^{inf}_{22}\ \boldsymbol{\sigma}^{inf}_{23}]$

According to these boundary conditions, the stress vanishes at infinity and a uniform traction t_T is applied to the upper crack surface and $-t_T$ is applied to the lower crack surface. Hence, the solution is given for these boundary conditions as :

$$u = Re\{ A \langle f(z_a) \rangle B^{-1} \} t_T \quad \text{(liv)}$$

$$\Phi = Re\{ B \langle f(z_a) \rangle B^{-1} \} t_T \quad \text{(lv)}$$

$$f(z_a) = (z_a^2 - a^2)^{0.5} - z_a \quad \text{(lv)}$$

Where,

A and B are normalized Stroh matrices defined in equations (xlvii) and (xlviii).

Using equations (xxxix) and (xl), the stresses are given by :

$t_1 = [\ \boldsymbol{\sigma}_{11}\ \boldsymbol{\sigma}_{12}\ \boldsymbol{\sigma}_{13}\ ]^T$

$$t_1 = -Re\{ B \langle f_{,2}(z_a) \rangle B^{-1} \} t_T \quad \text{(lvi)}$$

$t_2 = [\ \boldsymbol{\sigma}_{21}\ \boldsymbol{\sigma}_{22}\ \boldsymbol{\sigma}_{23}\ ]^T$

$$t_2 = Re\{ B \langle f_{,1}(z_a) \rangle B^{-1} \} t_T \quad \text{(lvii)}$$

The stress intensity factors at crack tips are :

$$K = (\pi . a)^{0.5} t_T \qquad \text{(lviii)}$$

Performing coordinate transformation at near crack tip solution to polar coordinates and shifting the origin to (a,0,0),

$$z_a = r . (\cos\theta + p_a \sin\theta) + a \qquad \text{(lix)}$$

This gives us, as r approaches 0,

$$f^a_{,1} (z_a) = (a / 2 . r (\cos\theta + p_a \sin\theta))^{0.5} \qquad \text{(lx)}$$

$$f^a_{,2} (z_a) = (p_a . a / 2 . r (\cos\theta + p_a \sin\theta))^{0.5} \qquad \text{(lxi)}$$

The θ dependence of the stress components in the cylindrical - polar coordinates as r approaches 0 for pure mode K_a loading. We obtain the asymptotic limit for the stress intensity factors from equation (lviii),

$$t^a_1 = -\mathrm{Re} \{B < p_a / (\cos\theta + p_a \sin\theta)^{0.5} > B^{-1} \} K \qquad \text{(lxii)}$$

$$t^a_2 = -\mathrm{Re} \{B < 1 / (\cos\theta + p_a \sin\theta)^{0.5} > B^{-1} \} K \qquad \text{(lxiii)}$$

Bibliography

[1] Yeh, J.-W.; Chen, S.-K.; Lin, S.-J.; Gan, J.-Y.; Chin, T.-S.; Shun, T.-T.; Tsau, C.-H.; Chang, S.-Y. (May 2004). "Nanostructured High-Entropy Alloys with Multiple Principal Elements: Novel Alloy Design Concepts and Outcomes". Advanced Engineering Materials. 6 (5): 299–303. doi:10.1002/adem.200300567. ISSN 1438-1656. S2CID 137380231

[2] Otto, F.; Yang, Y.; Bei, H.; George, E.P. (April 2013). "Relative effects of enthalpy and entropy on the phase stability of equiatomic high-entropy alloys". Acta Materialia. 61 (7): 2628–2638. Bibcode:2013AcMat..61.2628O. doi:10.1016/j.actamat.2013.01.042

[3] Zou, Yu; Maiti, Soumyadipta; Steurer, Walter; Spolenak, Ralph (February 2014). "Size-dependent plasticity in an Nb25Mo25Ta25W25 refractory high-entropy alloy". Acta Materialia. 65: 85–97. Bibcode:2014AcMat..65...85Z. doi:10.1016/j.actamat.2013.11.049. S2CID 137229215

[4] Gali, A.; George, E.P. (August 2013). "Tensile properties of high- and medium-entropy alloys". Intermetallics. 39: 74–78. doi:10.1016/j.intermet.2013.03.018

[5] Yeh, Jien-Wei (December 2013). "Alloy Design Strategies and Future Trends in High-Entropy Alloys". JOM. 65 (12): 1759–1771. Bibcode:2013JOM....65l1759Y. doi:10.1007/s11837-013-0761-6. ISSN 1047-4838. S2CID 255409483.

[6] Eleanor Mak, Binglun Yin, W.A. Curtin, “A ductility criterion for bcc high entropy alloys”, Journal of the Mechanics and Physics of Solids, Volume 152, 2021, 104389, ISSN 0022-5096

[7] Prashant Singh, Brent Vela, Gaoyuan Ouyang, Nicolas Argibay, Jun Cui, Raymundo Arroyave, Duane D. Johnson, “A ductility metric for refractory-based multi-principal-element alloys”, Acta Materialia, Volume 257, 2023, 119104, ISSN

1359-6454
[8] Yong-Jie Hu, Aditya Sundar, Shigenobu Ogata, Liang Qi, Screening of generalized stacking fault energies, surface energies and intrinsic ductile potency of refractory multicomponent alloys, Acta Materialia, Volume 210, 2021, 116800, ISSN 1359-6454
[9] Nathan Linton, Dilpuneet S. Aidhy; A machine learning framework for elastic constants predictions in multi-principal element alloys. APL Mach. Learn. 1 March 2023; 1 (1): 016109. https://doi.org/10.1063/5.0129928
[10] Pugh, S. F. (1954). XCII. Relations between the elastic moduli and the plastic properties of polycrystalline pure metals. The London, Edinburgh, and Dublin Philosophical Magazine and Journal of Science, 45(367), 823–843. https://doi.org/10.1080/14786440808520496
[11] R.P. Thompson, W.J. Clegg, Predicting whether a material is ductile or brittle, Current Opinion in Solid State and Materials Science, Volume 22, Issue 3, 2018, Pages 100-108, ISSN 1359-0286
[12] Senkov, O.N., Miracle, D.B. Generalization of intrinsic ductile-to-brittle criteria by Pugh and Pettifor for materials with a cubic crystal structure. Sci Rep 11, 4531 (2021). https://doi.org/10.1038/s41598-021-83953-z
[13] Pettifor DG. Theoretical predictions of structure and related properties of intermetallics. Materials Science and Technology. 1992;8(4):345-349. doi:10.1179/mst.1992.8.4.345
[13] Pierre Hirel, Atomsk: A tool for manipulating and converting atomic data files, Computer Physics Communications, Volume 197, 2015, Pages 212-219, ISSN 0010-4655, https://doi.org/10.1016/j.cpc.2015.07.012.
[14] G. Kresse and J. Hafner, Phys. Rev. B 47 , 558 (1993); ibid. 49 , 14 251 (1994).
[15] G. Kresse and J. FurthmÃ¼ller, Comput. Mat. Sci. 6 , 15 (1996).
[16] G. Kresse and J. FurthmÃ¼ller, Phys. Rev. B 54 , 11 169 (1996).

Where appropriate, the use of the data-base on ultrasoft pseudopotentials should be referenced as
[17] G. Kresse and J. Hafner, J. Phys.: Condens. Matt. 6, 8245 (1994).
If the PAW-version is used, an additional reference should be made to
[18] G. Kresse and D. Joubert, Phys. Rev. 59 , 1758 (1999).
[19] V. Wang, N. Xu, J.C. Liu, G. Tang, W.T. Geng, VASPKIT: A User-Friendly Interface Facilitating High-Throughput Computing and Analysis Using VASP Code, Computer Physics Communications 267, 108033 (2021). https://doi.org/10.1016/j.cpc.2021.108033
[20] Anubhav Jain, Shyue Ping Ong, Geoffroy Hautier, Wei Chen, William Davidson Richards, Stephen Dacek, Shreyas Cholia, Dan Gunter, David Skinner, Gerbrand Ceder, Kristin A. Persson; Commentary: The Materials Project: A materials genome approach to accelerating materials innovation. APL Mater. 1 July 2013; 1 (1): 011002. https://doi.org/10.1063/1.4812323
[21] Ting, T.T.C., 1996. Anisotropic elasticity: Theory and applications. In: Oxford Engineering Science Series, Oxford University Press, Oxford, New York.
[22] O. El-Atwani, N. Li, M. Li, A. Devaraj, J. K. S. Baldwin, M. M. Schneider, D. Sobieraj, J. S. Wróbel, D. Nguyen-Manh, S. A. Maloy, E. Martinez, Outstanding radiation resistance of tungsten-based high-entropy alloys. Sci. Adv. 5, eaav2002 (2019).
[23] Griffith Alan Arnold 1921VI. The phenomena of rupture and flow in solidsPhilosophical Transactions of the Royal Society of London. Series A, Containing Papers of a Mathematical or Physical Character221163–198 http://doi.org/10.1098/rsta.1921.0006
[24] Dislocation Nucleation from a Crack Tip: An Analysis Based on the Peierls Concept December 1992 Journal of the Mechanics and Physics of Solids 40(2):239-271 December 1992 40(2):239-271 DOI:10.1016/S0022-5096(05)80012-2

[25] Y.X. Ye, C.Z. Liu, H. Wang, T.G. Nieh, Friction and wear behavior of a single-phase equiatomic TiZrHfNb high-entropy alloy studied using a nanoscratch technique, Acta Materialia, Volume 147, 2018, Pages 78-89, ISSN 1359-6454, https://doi.org/10.1016/j.actamat.2018.01.014.
[26] Saad Sheikh, Samrand Shafeie, Qiang Hu, Johan Ahlström, Christer Persson, Jaroslav Veselý, Jiří Zýka, Uta Klement, Sheng Guo; Alloy design for intrinsically ductile refractory high-entropy alloys. J. Appl. Phys. 28 October 2016; 120 (16): 164902. https://doi.org/10.1063/1.4966659
[27] The Alloy-Theoretic Automated Toolkit (ATAT): A User Guide Axel van de Walle December 6, 2023.
[28] Xiaoqing Li, Wei Li, Douglas L. Irving, Lajos K. Varga, Levente Vitos, Stephan Schönecker, Ductile and brittle crack-tip response in equimolar refractory high-entropy alloys, Acta Materialia, Volume 189, 2020, Pages 174-187, ISSN 1359-6454, https://doi.org/10.1016/j.actamat.2020.03.004.
[29] Chemical short-range order in derivative Cr–Ta–Ti–V–W high entropy alloys from the first-principles thermodynamic study Damian Sobieraj, Jan S. Wróbel, Tomasz Rygier, Krzysztof J. Kurzydłowski, Osman El Atwani, Arun Devaraj, Enrique Martinez Saezd and Duc Nguyen-Manh Phys. Chem. Chem. Phys., 2020,22, 23929-23951
[30] Xue-Chun Zhang, Shuo Cao, Lian-Ji Zhang, Rui Yang, Qing-Miao Hu, Unstable stacking fault energy and peierls stress for evaluating slip system competition in body-centered cubic metals, Journal of Materials Research and Technology, Volume 22, 2023, Pages 3413-3422, ISSN 2238-7854, https://doi.org/10.1016/j.jmrt.2022.12.162.
[31] Priyanka Kumari, Amit K. Gupta, Rajesh K. Mishra, M.S. Ahmad, Rohit R. Shahi, A Comprehensive Review: Recent Progress on Magnetic High Entropy Alloys and Oxides, Journal of Magnetism and Magnetic Materials, Volume 554, 2022, 169142, ISSN 0304-8853, https://doi.org/10.1016/j.jmmm.2022.169142.

[32] George, E.P., Raabe, D. & Ritchie, R.O. High-entropy alloys. Nat Rev Mater 4, 515–534 (2019). https://doi.org/10.1038/s41578-019-0121-4
[33] A. Stukowski, Visualization and analysis of atomistic simulation data with OVITO - the Open Visualization Tool, Modelling Simul. Mater. Sci. Eng. 18 (2010), 015012
[34] Fernández-Caballero, A., Wróbel, J.S., Mummery, P.M. et al. Short-Range Order in High Entropy Alloys: Theoretical Formulation and Application to Mo-Nb-Ta-V-W System. J. Phase Equilib. Diffus. 38, 391–403 (2017). https://doi.org/10.1007/s11669-017-0582-3
[35] Juliusz Dąbrowa, Marek Zajusz, Witold Kucza, Grzegorz Cieślak, Katarzyna Berent, Tomasz Czeppe, Tadeusz Kulik, Marek Danielewski, Demystifying the sluggish diffusion effect in high entropy alloys, Journal of Alloys and Compounds, Volume 783, 2019, Pages 193-207, ISSN 0925-8388, https://doi.org/10.1016/j.jallcom.2018.12.300.
[36] Otto, F., Yang, Y., Bei, H., & George, E. P. (2013). Relative effects of enthalpy and entropy on the phase stability of equiatomic high-entropy alloys. https://doi.org/10.1016/j.actamat.2013.01.042
[37] O. El-Atwani, N. Li, M. Li, A. Devaraj, J. K. S. Baldwin, M. M. Schneider, D. Sobieraj, J. S. Wróbel, D. Nguyen-Manh, S. A. Maloy, E. Martinez, Outstanding radiation resistance of tungsten-based high-entropy alloys. Sci. Adv. 5, eaav2002 (2019).
[38] Owais Ahmed Waseem, Junho Lee, Hyuck Mo Lee, Ho Jin Ryu, The effect of Ti on the sintering and mechanical properties of refractory high-entropy alloy TixWTaVCr fabricated via spark plasma sintering for fusion plasma-facing materials, Materials Chemistry and Physics, Volume 210, 2018, Pages 87-94, ISSN 0254-0584, https://doi.org/10.1016/j.matchemphys.2017.06.054.